DESIGN, ANALYSIS, AND IMPLEMENTATION OF CIRCULAR DISK - ANNULAR RING (CDAR) ANTENNA

A THESIS SUBMITTED TO
THE GRADUATE SCHOOL OF NATURAL AND APPLIED SCIENCES
OF
MIDDLE EAST TECHNICAL UNIVERSITY

BY

MUSTAFA SANCAY KIRIK

IN PARTIAL FULFILMENT OF THE REQUIREMENTS
FOR
THE DEGREE OF MASTER OF SCIENCE
IN
ELECTRICAL AND ELECTRONICS ENGINEERING

DECEMBER 2007

DESIGN, ANALYSIS, AND IMPLEMENTATION OF CIRCULAR DISK - ANNULAR RING (CDAR) ANTENNA

submitted by **MUSTAFA SANCAY KIRIK** in partial fulfillment of the requirements for the degree of **Master of Science in Electrical and Electronics Engineering Department, Middle East Technical University** by,

Prof. Dr. Canan ÖZGEN
Dean, Graduate School of Natural and Applied Sciences _____

Prof. Dr. İsmet ERKMEN
Head of Department, Electrical and Electronics Engineering _____

Assoc.Prof. Dr. S. Sencer KOÇ
Supervisor, Electrical and Electronics Engineering Dept., METU _____

Examining Committee Members:

Prof. Dr. Altunkan HIZAL
Electrical and Electronics Engineering Dept., METU _____

Assoc.Prof. Dr. S. Sencer KOÇ
Electrical and Electronics Engineering Dept., METU _____

Prof. Dr. Gülbin DURAL
Electrical and Electronics Engineering Dept., METU _____

Assoc.Prof. Dr. Özlem Aydın ÇİVİ
Electrical and Electronics Engineering Dept., METU _____

Dr. Özlem ŞEN
Chief Researcher, TÜBİTAK-UZAY _____

Date: 13.12.2007

I hereby declare that all information in this document has been obtained and presented in accordance with academic rules and ethical conduct. I also declare that, as required by these rules and conduct, I have fully cited and referenced all material and results that are not original to this work.

Name, Last name : MUSTAFA SANCAY KIRIK

Signature :

ABSTRACT

DESIGN, ANALYSIS, AND IMPLEMENTATION OF CIRCULAR DISK - ANNULAR RING (CDAR) ANTENNA

KIRIK, Mustafa Sancay
M.S., Department of Electrical and Electronics Engineering
Supervisor : Assoc. Dr. S. Sencer KOÇ

December 2007, 102 pages

In satellite applications, a circularly polarized satellite antenna is desirable with a pattern that results in constant received power while the distance between the transmitter and the receiver is changing. The Circular Disk - Annular Ring (CDAR) antenna satisfies these requirements along with other requirements for the satellite antenna. The CDAR antenna is a combination of a Circular Disk and an Annular Ring patch antennas. In this thesis, a circularly polarized CDAR antenna that is fed from a single point is designed at the center frequency of 8.2 GHz. This antenna is investigated and optimized to ease the fabrication process. The design parameters are defined on this report and optimized by using an Electromagnetic Simulation software program. In order to verify the theoretical results, Circular Disk - Annular Ring Antenna is produced as a prototype. Measurements of antenna parameters, electromagnetic field and circuit properties are interpreted to show compliance with theoretical and simulation results. The values of deviation between theoretical and experimental results are also discussed.

Keywords: Satellite Antenna, Singly-fed Circular Polarization, Antenna Pattern, Circular Disk Patch Antenna, Annular Ring Patch Antenna, Antenna Feeding

ÖZ

DİSK - HALKA (CDAR) ANTENİN TASARIMI, İNCELENMESİ VE UYGULANMASI

KIRIK, Mustafa Sancay
Yüksek Lisans, Elektrik-Elektronik Mühendisliği Bölümü
Tez Yöneticisi: Doç. Dr. S. Sencer KOÇ

Aralık 2007, 102 Sayfa

Uydu uygulamalarında, verici ve alıcı antenlerin arasındaki uzaklığın değişmesi sebebiyle, sabit güç paterni sağlayan dairesel polarizasyonlu antenler tercih edilmektedir. Disk - Halka (CDAR) yama anten, bu gereksinimleri uydu antenlerinin diğer gereksinimleri ile birlikte karşılamaktadır. Disk - Halka anten, bir dairesel disk yama anten ve bir halka yama antenin birleşiminden oluşmaktadır. Bu tezde, 8.2 GHz merkez frekansında, tek noktadan beslenen dairesel polarizasyona sahip Disk - Halka anten tasarımı gerçekleştirilmiştir. Bu antenin tasarım parametreleri, üretim işlemlerini kolaylaştırabilmek için araştırılmış ve en uygun anten değerleri tespit edilmiştir. Bu rapordaki tasarım parametrelerinin en uygun değerleri, elektromanyetik simülasyon programı kullanılarak belirlenmiştir. Teorik sonuçları doğrulamak amacıyla Disk - Halka anten prototip olarak üretilmiş ve ölçümleri yapılmıştır. Ölçülen anten parametreleri, elektromanyetik alan ve devre özellikleri, teorik ve simülasyon sonuçlar ile yorumlanarak, bunlar arasındaki uyum gözlenmiştir. Tasarlanan ve ölçülen değerler arasındaki farklar da sonuç kısmında incelenmiştir.

Anahtar kelimeler: Uydu Anteni, Tek Noktadan Belenen Dairesel polarizasyon, Anten Paterni, Dairesel Disk Yama Anten, Halka Yama Anten, Anten Beslemesi

To FERİHA

ACKNOWLEDGEMENTS

I would like to express my gratitude to Assoc. Dr. S. Sencer KOÇ for his precious supervision, helpful guidance and frank interest throughout all the phases of this study. This thesis bears valuable importance to me for the fact that I had found the chance to work with him.

I would also like to acknowledge Dr. Orhan ŞENGÜL for very constructive suggestion and support during the course of the thesis

TABLE OF CONTENTS

LIST OF TABLES

LIST OF FIGURES

CHAPTER 1

INTRODUCTION

1.1. A Literature Survey on Satellite Antennas

Communication system is a crucial part of a satellite, because after the launch of the system, it will be the only facility that provides communication between the ground station and the satellite. As satellites have limited power, the communication system like all other systems of the satellite should use the power efficiently. However due to severe link budget requirements, to satisfy a reliable communication with limited power, space antenna should have a radiation pattern that results in constant received power while the distance between the transmitter and the receiver is changing.

In RASAT (Low Earth Orbit (LEO) Satellite being designed in TUBITAK-UZAY), communication starts at ±15° from the earth surface. LEO satellites have very limited power, and at ±15° degrees above the horizon, they have a severe link budget. Therefore to provide a reliable communication link between such LEO satellites, the communication system has to satisfy the link budget requirements by using appropriate ground station antenna. The major principle behind the reliable communication by appropriate ground station antenna is the logarithmic "power budget" equation that defines a communication link's performance. In this power budget equation, the transmitting and receiving antenna gains and the transmitter power are all effective. But one can not increase the transmitter power due to limited power of satellites, so the transmitter antenna should have maximum gain in order not to increase the size of ground station antenna. Also to satisfy the required link budget, this gain should be directed efficiently. The main idea is that at 90 degrees from the earth surface (that means the satellite is just above the ground station), the distance between the satellite and

the ground station is minimum, which implies that smaller antenna gain is enough. On the contrary, when the satellite is at a position of ±15° above the horizon, the link budget requirements get severe and more transmit antenna gain is needed. We can formulate this situation as follows:

The received power by ground station antenna P_r is:

$$P_r = \frac{G_s P_s}{4\pi r^2} A_e$$

where

$$A_e = \frac{\lambda^2}{4\pi} G_e$$

then we can write

$$P_r = \left(\frac{\lambda}{4\pi r} \right)^2 G_e G_s P_s$$

where

G_e = Gain of the ground station antenna

G_s = Gain of the transmitter antenna

P_s = Power of the transmitter antenna

r = Distance between the satellite and the ground station

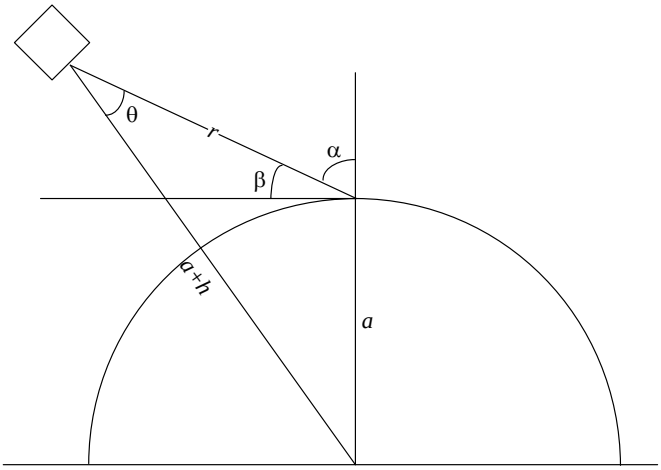

Figure 1-1: Satellite and Earth Geometry

Figure 1-1 shows the satellite position with respect to the Earth. In the figure, "h" is the height of the satellite from earth, "θ" is the angle of ground station with respect to the satellite antenna, "r"is the distance between the satellite and the ground station and "a" is the radius of the earth. According to this figure, the distance "r" and the angle "θ" are changing, and to keep the received power P_r constant:

$$\frac{G_s}{r^2} = Constant$$

should be satisfied.

Since the earth radius "a" is much greater than the satellite distance "h", one can assume that the transmitter antenna which has a secant-squared power pattern will satisfy the constant received power requirements. The secant-squared power pattern can be expressed as:

$$G_s(\theta) = G(0)\sec^2(\theta) \qquad \text{for } 0 < \theta < \theta_m$$

where θ is the elevation angle and θ_m is the angle above which the pattern no more resembles the secant-squared equation [2].

On the other hand, because the location of the satellite is changing with respect to the ground station, using circularly polarized antennas typically adds 3dB to the link margin, compared to linear polarized antennas. Otherwise ground station antenna should be rotated for polarization match, which results in complex ground station antenna tracking system.

1.2. Brief History of Thesis Study

Microstrip antennas, single-feed circular polarization, power dividers and couplers are the main subject of this thesis study. The goal of this thesis is to design and implement single-feed circularly polarized microstrip antenna structure that satisfies the secant-square power pattern for LEO satellites X-Band communication system. The design steps are listed below which are the main topics discussed in the chapters of this thesis.

1. A literature survey on satellite antennas
2. Microstrip Patch Antennas and their excitation modes
3. Circular Polarization techniques
4. Feeding techniques and structures for patch antennas
5. Power Dividers and Couplers
6. CDAR antenna design and simulation results
7. Test results and verification of simulation results

The first chapter is composed of the literature survey of LEO satellite communication system. The main idea and requirements of the transmitter antenna system are given in this chapter.

In the second chapter, investigation of basic circular disk and annular ring type antennas with their dominant and higher order mode excitations is the main concern. Also appropriate mode excitations of these two antenna elements to satisfy the requirements of X-Band transmitter antenna CDAR, is discussed. The selection of mode excitations is facilitated by considering the mode patterns of radiating patches.

Thirdly, because circular polarization is one of the most important aspects of CDAR antenna design, different types of circular polarization techniques are discussed. To simplify the manufacturing process, mainly single feed circular polarization techniques are considered.

In the fourth chapter, appropriate feeding structures are studied. Advantages and disadvantages of various types of feeding structures are investigated, and the one most suitable for the purpose is discussed.

Chapter five deals with the distribution of the power between circular disk and annular ring patch antennas. Different types of power dividers and couplers are investigated and discussions on their advantages and disadvantages are included.

The sixth chapter is the main part in which the CDAR antenna implementation and simulation results are studied. This section starts with design of separate antenna elements at resonant frequencies and continues with superposition of radiating patches, implementation of single feed circular polarization technique, designing the appropriate 10 dB broadside coupler and analyzing the simulation results of whole system.

Finally, the measurement results are analyzed and the simulation and measurement results are compared.

To sum up, in the following chapters, design, implementation and measurement of LEO satellite X-band transmitter antenna is studied and discussed by comparing the simulation and measurement results.

CHAPTER 2

MICROSTRIP PATCH ANTENNAS

The CDAR antenna is a combination of a Circular Disk and an Annular Ring patch antennas. The design process of the CDAR antenna starts with investigating single circular disk and annular ring patch radiators. This chapter explains the basic properties of microstrip antennas by giving their advantages and disadvantages. The design considerations, patch antenna parameters and their analytical expressions are also studied in this chapter. However, the calculated design parameters, and simulated results of the CDAR antenna are given in chapter 6.

2.1 Introduction to Microstrip Patch Antennas

Microstrip patch antennas are used commonly because of their simple fabrication techniques. They are also known as printed antennas and these antennas are often mounted on aircrafts, satellites, or receiving-transmitting applications where low power, low profile radiators are needed. They were invented in the 1950's and have become very popular in a relatively short span of one or two decades.

The simplest configurations of microstrip patch antennas consist of an antenna element as radiating patch bonded to a dielectric as insulator (generally $\varepsilon_r \leq 10$), and on the other side, the structure has a continuous metal layer as a ground plane.

The radiation principle is very similar to radiation of microstrip lines. The field distribution between the patch and the ground plane determines the radiation from a microstrip antenna. Another approach to radiation structure can be described as the surface current distribution on the patch. When the patch is fed, there exists a

charge distribution on the upper and lower surfaces, as well as on the surface of the ground plane.

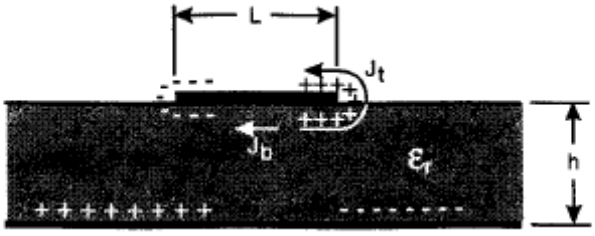

Figure 2-1: Current Distribution on Patch Antenna

The energization of the radiator will create a charge distribution on the upper and lower surfaces of the patch, as well as on the surface of the ground plane. There are repulsive forces between like charges and because of momentum of these charges; current densities J_b and J_t are created [Figure 2-2]. In the figure, h is the substrate thickness, w is the width of the patch and L is the length of the patch. For small h/w ratio, attractive force between charges leads that the current flows underneath the patch. So the patch can be modeled as a cavity which is a commonly used analytical model of the patch radiators.

The general characteristics of microstrip patch antennas can be summarized as:

- Size of patch is directly tied to the wavelength of resonant frequency.
- These antennas have a maximum directive gain of 6-9 dBi.
- Patch antennas usually have wide Beamwidth (3 dB bandwidth is at about 60 to 90 degrees.)
- Generally low dielectric constant and thick dielectric substrate is used for higher radiation efficiency and bandwidth.

The advantages and disadvantages of using microstrip patch antennas are listed below:

Advantages:

- Light weight, low volume, thin profile which can be fabricated and used very easily.
- Linear and circular polarizations are possible by changing the feeder structure.
- Dual frequency and dual polarization antennas are possible
- These antennas can easily be integrated to microwave integrated circuits.
- They are easy to manufacture and robust against small changes of parameters during production.

Disadvantages and limitations:

- Patch antennas have narrow bandwidth
- They have lower gain (6-9 dBi)
- Most microstrip antennas radiate into half-space
- Polarization purity is difficult to achieve
- Complex feeding structures are needed for higher performance
- Reduced gain and efficiency due to cross-polarization in array type antennas

2.2 Design Considerations for Microstrip Patch Antennas

Patch antennas can be designed in any shape, but some design limitations restricts the design, such as substrate dielectric constant, substrate thickness, feeding point and structure or finite ground plane size. These parameters are selected by regarding the gain, pattern or polarization structures of the antenna.

One of the first design steps is choosing the right substrate and substrate thickness. Thicker substrate will increase the radiated power and improve impedance bandwidth. Also it will be mechanically stronger. However, the dielectric loss, and unwanted radiation from the probe feed will increase. Similar situations are valid for dielectric constant. Low value of ε_r will increase the fringing field at the patch periphery, so the radiated power will increase. But the patch size will be bigger when a low ε_r substrate is used.

The second criterion of design procedure is feeding point location. The feeding point determines the characteristic impedance of feed. So, change in feeding point gives the opportunity to match the antenna feed to characteristic impedance. Also, feeding point is effective in polarization. Especially in single feed circular polarization methods, feeding point determines the characteristics of the polarization.

2.3 Design and analysis of Circular Disk Microstrip Antenna

Circular Disk Microstrip Patch antenna is one of the simplest patch configurations. There are various models for analyzing the circular disk patches such as: cavity model, mode matching with edge admittance, transmission line model and Finite Difference Time Domain (FDTD). For thin substrates, cavity model and transmission line model are valid because the variation of the field among the substrate thickness is negligible. The cavity model is analyzed as follows [3, 4]:

The electric field in the cavity should satisfy the wave equation along with the boundary conditions.

$$(\nabla^2 + k^2)\vec{E} = 0 \qquad k = 2\pi\sqrt{\frac{\varepsilon_r}{\lambda_0}}$$

The TM solutions of this equation for cavity model in cylindrical coordinates:

$$E_z = E_0 J_n(\frac{x_{nm}}{a}\rho)\cos n\phi$$

where J_n is the Bessel function of order n, x_{nm} is the mth zero of the function $J_n(z)$ which comes from the boundary conditions of cavity model, and "a" is the radius of the circular disk patch. At resonant frequency, one has:

$$k = \frac{x_{nm}}{a}.$$

For TM mode numbers "$n = m = 1$", which is known as the "Dominant Mode", the patch has minimum radius at resonant frequency. The field expressions for this mode can be written as:

$$E_z = E_0 J_1(\frac{x_{11}}{a}\rho)\cos\phi$$

$$H_\rho = -J_\phi = -\frac{j}{\omega\mu\rho}E_0 J_1(\frac{x_{11}}{a}\rho)\sin\phi$$

$$H_\phi = J_\rho = -\frac{jk}{\omega\mu}E_0 J_1(\frac{x_{11}}{a}\rho)\cos\phi$$

The design parameters of circular disk radiator and their analytical expressions are listed below.

- **Resonant Frequency**

From the equation:

$$x_{nm} = ka,$$

the resonant frequency of TM_{nm} mode can be found as:

$$f_{nm} = \frac{x_{nm} c}{2\pi a \sqrt{\varepsilon_r}}$$

where

"c" is the speed of light in free space,

"a" is the radius of circle,

"f_{nm}" is the resonant frequency,

"ε_r" is the dielectric constant of dielectric substrate,

"$x_{nm} = k_{nm} a$" is the root of characteristic equation at TM_{nm} mode

First 5 roots of the derivative of Bessel Functions are given in Table 2-1.

Table 2-1: Roots of Bessel Derivative Function

m \ n	0	1	2	3	4
1	0	1.84118	3.05424	4.20119	5.317
2	3.38171	5.331			

Because of the fringing fields along the edges, substrate thickness affects the resonant frequency. This effect can be taken into account by defining an effective radius "a_e" as [3, 4]:

$$a_e = a\left\{1 + \frac{2h}{\pi * a \varepsilon_r}\left(\ln\frac{\pi * a}{2h} + 1.7726\right)\right\}^{\frac{1}{2}}$$

This effective radius expression is used instead of circular disk antenna radius expression given before.

- **Radiation Patterns**

For the Dominant TM_{11} mode, the radiation characteristics of circular disk, obtained from cavity model are [3]:

$$E_\theta = -jV\frac{ak_0}{2}\frac{e^{-jk_0r}}{r}\cos\phi J_1(k_0 a\sin\theta)$$

$$E_\phi = jV\frac{ak_0}{2}\frac{e^{-jk_0r}}{r}\frac{J_1(k_0 a\sin\theta)}{k_0 a\sin\theta}\cos\theta\sin\phi$$

where

$V = hE_1 J_1(k_{nm}a)$ is the edge voltages at $\phi = 0$.

- **Radiated Power**

The radiated power may not be considered as a design parameter. However the given expression is used in calculating the feeding point location. The radiated power of the circular disk patch can be found by integrating the pointing vector over the hemisphere above the disk [3]. The radiated power is:

$$P_r = \frac{1}{2\eta_0}\int_0^{2\pi}\int_0^{\pi/2}\left(\left|E_\theta\right|^2 + \left|E_\phi\right|^2\right)r^2\sin\theta d\theta d\phi$$

Then using the serial expansion of Bessel Function, for $n = 1$ mode, the radiated power expression will be:

$$P_r = \frac{(E_0 H)^2 \pi^3 a^2}{2\lambda_0^2 \eta_0}\left[\frac{4}{3} - \frac{8}{15}(k_0 a)^2 + \frac{11}{105}(k_0 a)^4 - \ldots\right]$$

- **Directivity and Gain**

The directivity can be defined as maximum power density in the main lobe to the average power density. The directivity of a circular disk can be written as:

$$D = \frac{\frac{1}{2}\mathrm{Re}\left(E_\theta H_\phi^* - E_\phi H_\theta^*\right)_{\theta=0}}{P_r / 4\pi * r^2}$$

The gain is directly related to the directivity. Gain of the antenna is multiplication of directivity and radiation efficiency. The radiation efficiency is defined as the ratio of radiated power to the input power. Because radiation efficiency is always less than 1, the gain is also less than directivity.

- **Feeding Point**

The feeding point is an important design consideration to satisfy the matching condition of the input impedance. The feeding point depends on the radiation resistance and Bessel Function square. In TM_{11} mode, the input resistance R_{in} can be calculated from radiation resistance R_r by equating the following expression to the matching condition (50 Ω):

$$R_{in} = R_r \frac{J_1^2(k_{11}\rho_0)}{J_1^2(k_{11}a)}$$

where

$$k_{11} = \frac{x'_{11}}{a}$$

$$R_r = 1/G_r = \frac{(E_0 h)^2}{2P_r}$$

In which, P_r is the radiated power given before, [3].

- **Dielectric Constant and Substrate Thickness**

As a general rule, the substrate should have low dielectric constant for better radiation efficiency, and thick substrate to increase the bandwidth.

When higher dielectric constant substrate is used in circular disk, the pattern of the dominant mode broadens, but the symmetry of the pattern will be lost. This leads to an increase in cross-polarization [3, 4 and 12].

Thicker substrates also affect the circular disk patch. Beside the increase in bandwidth, the resonant frequency will be shifted because of the fringing effect at the edge of the patch.

2.4 Design and analysis of Annular Ring Microstrip Antenna

Various shape of Ring microstrip patch antennas such as: circular, rectangular, square and triangular etc. have been studied in the literature. There are several interesting features about these antenna types. First of all, the size of the ring patch is more compact than the disk antenna at a given resonant frequency at TM_{11} dominant mode. This feature gives the opportunity that one can design more compact antenna arrays. Secondly, separation of the resonant modes can be controlled by the radius of inner and outer circle radii. This implies that the bandwidth of higher order mode such as TM_{12} is several times larger than the bandwidth of other patch antennas. Lastly, the annular ring antennas can be easily combined with circular disk antenna for designing dual frequency antenna array.

The study discussed in this thesis resembles this feature, but (Circular Disk Annular Ring) CDAR antenna is a combination of a disk and a ring antenna at the same resonant frequency for achieving special power pattern.

The annular ring type of antenna can also be analyzed by cavity model as in the circular disk case. The cavity model of the ring is modeled by replacing its peripheries with magnetic walls. The solution of the wave equation acquired from cavity model is [4]:

$$E_z = E_0\left[J_n(k_{nm}\rho)Y'_n(k_{nm}a) - J'_n(k_{nm}a)Y_n(k_{nm}\rho)\right]\cos(n\phi)$$

All the field components except for E_z, H_ρ and H_ϕ vanishes inside the cavity. The surface current on the lower surface of the ring metallization goes to zero along the edges at $\rho = a$ and $\rho = b$ to satisfy the magnetic wall boundary condition.

$$J_\rho(\rho = a) = H_\phi(\rho = a) = 0 \text{ and } J_\rho(\rho = b) = H_\phi(\rho = b) = 0$$

From this expression; the boundary condition leads to the following characteristic equation which defines the resonant condition.

$$J'_n(kb)Y'_n(ka) - J'_n(ka)Y'_n(kb) = 0$$

The roots of the characteristic equation ($\chi_{nm} = k_{nm}a$) define the resonant frequencies of the ring patch. Table 2-2 gives first few roots of the characteristic equation for different modes and for different outer to inner radius ratios (b/a).

Table 2-2: Roots of Characteristic Equation ($\chi_{nm} = k_{nm} a$)

$\chi_{nm} = k_{nm} a$	TM11	TM12	TM13
$b/a = 2.1$	0.656586	3.00369	5.78542
$b/a = 2.3$	0.618632	2.5761	4.91264
$b/a = 2.5$	0.584713	2.26364	4.2733
$b/a = 2.7$	0.554172	2.02534	3.7849
$b/a = 2.8$	0.540007	1.92619	3.58156

The design parameters of annular ring radiator and their analytical expressions are listed below [4].

- **Resonant Frequency**

Approximate value of the inner radius at resonant frequency can be obtained from the cavity model:

$$f_{nm} = \frac{\chi_{nm} c}{2\pi a \sqrt{\varepsilon_r}}$$

where

"c" is the speed of light in free space

"a" is the radius of inner circle

"f_{nm}" is the resonant frequency

"ε_r" is the dielectric constant of dielectric substrate

"$\chi_{nm} = k_{nm} a$" is the root of characteristic equation for TM_{nm} mode

In this expression, the effect of the fringing fields exists because of the thickness of the dielectric substrate. The inner radius calculated by this formula is not at resonant frequency. To optimize this situation, effective dielectric constant is used.

To determine the ε_{re}, the ring resonator is modeled as a microstrip line bent in a circular shape [3,4]. The effect of the curvature on the resonant frequency, because of relatively high substrate thickness, can be added to effective dielectric constant ε_{re} as follows [4]:

$$\varepsilon_{re} = \frac{1}{2}(\varepsilon_r + 1) + \frac{1}{2}(\varepsilon_r - 1)(1 + \frac{10h}{W}^{1/2})$$

where

"h" is the thickness of dielectric substrate

"$W = b - a$"is the difference between outer and inner circle radii.

By using this effective radius, one can find the resonant inner radius of ring patch quite accurately. The accuracy is about at 3%. To improve this accuracy rate, the ring patch can be modeled by parallel plate model [3].

- **Radiation Pattern**

The radiation fields can be obtained analytically either from magnetic current approach or electric current distribution method. The calculation of magnetic currents are similar to circular disk ones, but in this case there are two magnetic

currents existing at $\rho = a$ and $\rho = b$. The electric field under the patch is given as [4]:

$$E_z = E_0\left[J_n(k_{nm}\rho)Y'_n(k_{nm}a) - J'_n(k_{nm}a)Y_n(k_{nm}\rho)\right]\cos(n\phi)$$

The far field radiation fields obtained from the magnetic current approach at $\rho = a$ and $\rho = b$, [3,4]:

$$E_{nm,\theta}(\theta,\phi) = j^n \frac{2E_0}{\pi k_{nm}} \frac{e^{-jk_0 r}}{r} k_0 h\left[J'_n(k_0 a\sin\theta) - \frac{J'_n(k_{nm}a)}{J'_n(k_{nm}b)} J'_n(k_0 b\sin\theta) \right]\cos(n\phi)$$

$$E_{nm,\phi}(\theta,\phi) = -nj^n \frac{2E_0}{\pi k_{nm}} \frac{e^{-jk_0 r}}{r} k_0 h\left[\frac{J_n(k_0 a\sin\theta)}{k_0 a\sin\theta} - \right.$$
$$\left. \frac{J'_n(k_{nm}a)}{J'_n(k_{nm}b)} \frac{J_n(k_0 b\sin\theta)}{k_0 b\sin\theta}) \right]\sin(n\phi)\cos(\theta)$$

As seen from the far field expressions, the radiation pattern only depends on the "n" mode number. The "m" value in TM_{nm} expression does not affect the phase of the radiation. In TM_{1m} modes, when m is odd, fringing fields at the inner and outer apertures are in opposite polarity. This opposite polarity of fringing fields leads to subtractive interference which causes less radiation at the odd modes. On the other hand, when m is even, the fringing fields are additive which causes increase in the radiation.

For radiation pattern, b/a ratio changes the directivity and side lobe levels. If b/a ratio increases, the beamwidth of radiation pattern decreases which leads to more directive patterns. Also increase in b/a ratio causes increase in side lobe levels. This ratio affects the size of the ring antenna. The ratio determines the roots of characteristic equation and inner and outer radii of the patch.

CHAPTER 3

CIRCULAR POLARIZATION TECHNIQUES

The CDAR antenna has to be circularly polarized to add 3 dB to the link budget. In this chapter, some of the most popular circular polarization techniques for patch antennas are investigated. The techniques may be divided into two groups. One group includes all the multi-point feed circular polarization techniques, and the other one consists of singly-fed circular polarization techniques. For easy assembly, the CDAR antenna is designed by using singly-fed circular polarization techniques. The singly-fed circular polarization design is one of the most important part of this thesis study. In the following chapter, all the polarization techniques and their analytical expressions are discussed and in chapter 6, the polarization technique used in the CDAR antenna and its calculated design parameters are studied.

3.1 Need of Circular Polarization

The circular polarization can be briefly described as; the electromagnetic wave is resolved into two linearly polarized waves, of equal amplitude, in phase quadrature (90 degrees apart) and with their planes of polarization at right angles to each other. The radiated wave travels between horizontal and vertical planes. If this rotation is in clockwise direction, it is called right hand circular polarization (RHCP), otherwise it is called left hand circularly polarization (LHCP).

Circular polarization is used in radio systems like: communication, navigation and radar systems. Usage of circular polarization has several advantages and these advantages are listed on this section. As the transmitter and the receiver antenna locations are not stationary in the satellite applications, radio signals coming from the transmitter antenna may not be received by the ground station receiver antenna

due to the polarization mismatch. Because circular polarization radiates and/or receives in all planes, the reflected signal strength will not be lost because of unmatched polarization. Thus one can claim that circular polarization typically adds 3 dB to the link budget; otherwise, the ground station has to rotate the receiver antenna for polarization match. This is the main reason of using circularly polarized antenna in satellite communication systems.

3.2 Multi-Point Feed Circularly Polarized Antennas

The simplest multi-point feed circular polarization technique is dual-orthogonal fed type. There is 90° angular spacing between two excitation points. With this spacing, the fields generated from the two feeds are orthogonal to each other under the patch as well as outside the patch. In addition, with this angular spacing, one probe is always situated in the null field region of the other probe, thus causing very little mutual coupling between the two probes [3, 4, 5].

The dual orthogonal feeds are excited with equal amplitude but 90° phase difference. In patch antennas, if two orthogonal modes are exited with equal amplitude but in phase difference, this leads the patch to radiate in circular polarization. However, for beam symmetry and lower cross polarization, unwanted higher excitation modes should be suppressed. To suppress the undesired modes, additional feeds can be added with locations diagonally symmetric to actual feed points. These four feeds should be exited with equal magnitude but 0°-90°-0°-90° phase difference for even order modes or 0°-90°-180°-270° phase difference for odd order modes (Figure 3-1). By this feeding structures, higher order undesired modes cancel each other. The far field radiation expressions including all 4 feed excitation will be [5]:

$$E_\theta^t = E_\theta^1(\phi,\theta) + jE_\theta^2(\phi+\alpha,\theta) + \mathrm{sgn}(n)\left[E_\theta^3(\phi+180,\theta) + jE_\theta^4(\phi+180+\alpha,\theta)\right]$$

$$E_\phi^t = E_\phi^1(\phi,\theta) + jE_\phi^2(\phi+\alpha,\theta) + \mathrm{sgn}(n)\left[E_\phi^3(\phi+180,\theta) + jE_\phi^4(\phi+180+\alpha,\theta)\right]$$

Where superscripts 1, 2, 3, 4 indicate the four probes and α indicates the feed angular spacing. In $\text{sgn}(n)$ function, "n" represents the mode number and is defined as $\text{sgn}(n) = +1$ for even mode orders and $\text{sgn}(n) = -1$ for odd mode orders.

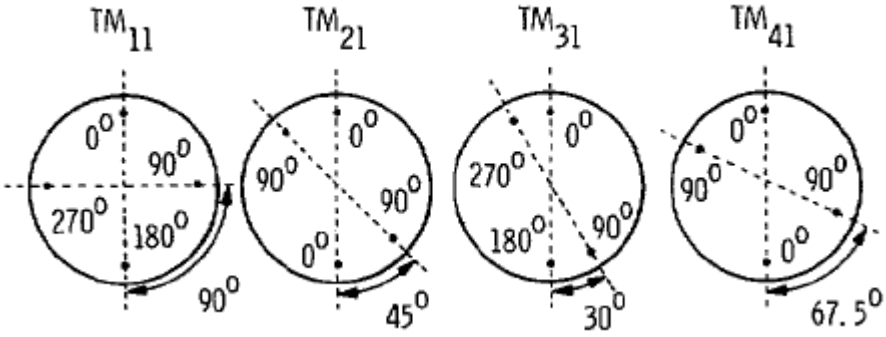

Figure 3-1: Four Probe Feed with Appropriate Angles and Phases

The multi point feeding technique is very common in circularly polarized patch antennas; however, a complex power dividing and feeding structure is required. These structures are usually harder to manufacture than singly-fed structures.

3.3 Singly-Fed Circularly Polarized Antennas

The basic idea to obtain circular polarization in patch antennas is to excite two orthogonal modes in equal amplitude and in-phase quadrature. In singly-fed circular polarization technique, patch surface is perturbed to achieve the excitation of orthogonal modes. When the patch radiator is fed from its input port, a generated mode is excited in an electrically thin cavity region of the patch. The generated mode is separated into two orthogonal modes by the effect of perturbation segments such as slots, truncated edges, etc. In Figure 3-2, the

truncated edges, amplitude and phase graphics are shown. At resonant frequency, the two orthogonal modes are in equal magnitude and in phase quadrature.

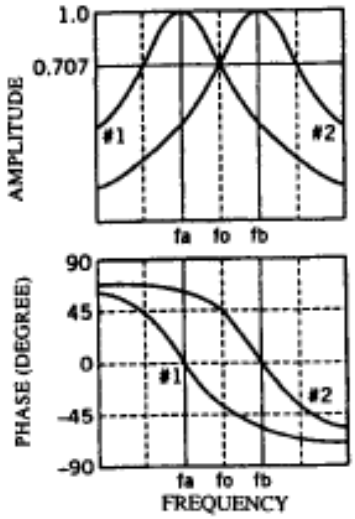

Figure 3-2: Amplitude and Phase of Orthogonal Modes in Singly-Fed Circularly Polarized Antenna

Various types of perturbation segments can be constituted. The main criteria of perturbation segments are the perturbation segment area, and the location of the feed point. The feed point should always be located diagonal to perturbation segments. This location also affects the circular polarization type. If the feed is on the right side of the diagonal, the patch radiates in RHCP, otherwise it radiates in LHCP. The perturbation area ΔS causes the dominant mode TM_{110} to be separated into two orthogonal degenerate modes. The perturbation segment area shifts the resonant frequency and the other design parameters. The pertinent expressions are, [3]:

Table 3-1: Expressions for Singly-Fed Circular Polarization

$f_a = f_{0r}(1+0.4185\frac{\Delta S}{S})$	$L_a = \frac{1}{(w_a^2 C_0)}$
$f_b = f_{0r}(1-0.4185\frac{\Delta S}{S})$	$L_b = \frac{1}{(w_b^2 C_0)}$
$N_a = K\cos(\phi_F + 45^0)$	$G_a = \frac{w_a C_0}{(Q_{0a})}$
$N_b = K\sin(\phi_F + 45^0)$	$G_b = \frac{w_b C_0}{(Q_{0b})}$
$K = \sqrt{2}\sqrt{\frac{x_{11}^2}{x_{11}^2 - 1}}\left(\frac{J_1(\frac{x_{11}\rho_0}{a})}{J_1(x_{11})}\right)$	$C_0 = \frac{\varepsilon S}{t}$
$x_{11} = 1.841$	$Y_a = G_a + j(wC_0 - \frac{1}{wL_a})$
$Q_0 = Q_a = Q_b$	$Y_b = G_b + j(wC_0 - \frac{1}{wL_b})$

The x_{11} is the root of first order Bessel Functions for dominant mode TM_{11} and Q_0 is the unloaded quality factor of the circular patch. The ratio $\frac{V_a}{V_b}$ can be written as:

$$\frac{V_b}{V_a} = \left(\frac{N_b}{N_a}\right)\left(\frac{Y_a}{Y_b}\right) = \left(\frac{N_b}{N_a}\right)\frac{\left\{\frac{f_a}{Q_0} + j\left(f - \frac{f_a^2}{f}\right)\right\}}{\left\{\frac{f_b}{Q_0} + j\left(f - \frac{f_b^2}{f}\right)\right\}}.$$

For circular polarization $\frac{V_b}{V_a} = \pm j$ should be satisfied and if the turn ratio ($\frac{N_a}{N_b}$) is selected as unity, after some simplifications, the ratio of perturbed area to all patch area $\frac{\Delta S}{S}$ can be calculated as:

$$\frac{\Delta S}{S} = \frac{1}{x_{11} Q_0}.$$

Various types of perturbation for circular patches are shown in Figure 3-4.

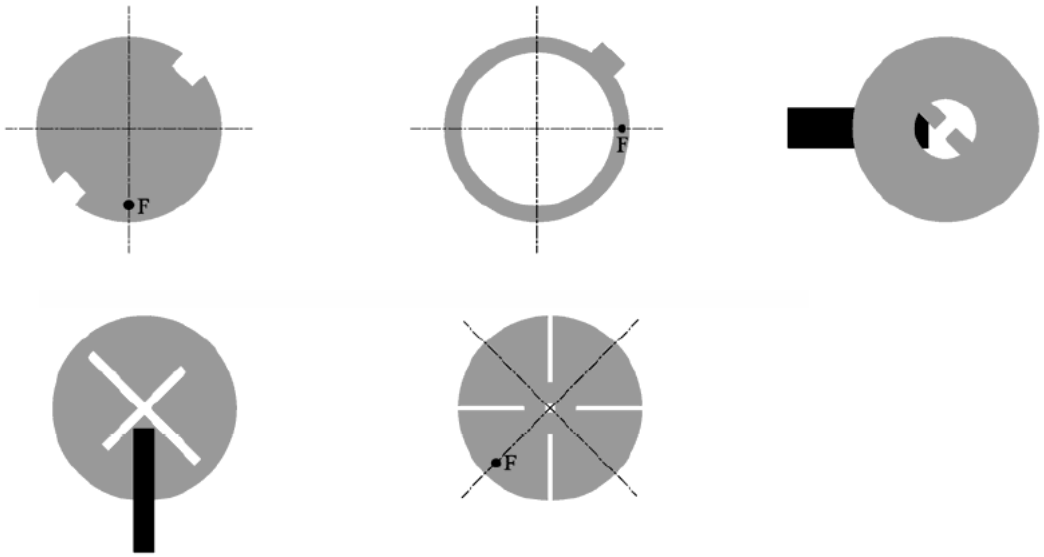

Figure 3-3: Different Configurations of Perturbation Segments

CHAPTER 4

FEEDING TECHNIQUES and STRUCTURES

There are plenty of ways to excite a microstrip antenna. Since the excitation method can affect the antenna radiation characteristics, it is a crucial part of an antenna system. The best feeding method can be decided by considering all the issues such as; type of the antenna, power divider circuit and manufacturing process. This chapter explains most of the popular feeding structures used in microstrip patch antennas. The advantages and disadvantages of different feeding methods and the design considerations of these feeding structures are investigated. What kind of feeding structure is chosen, and the reason why it is used in CDAR antenna is also studied at the end of this chapter.

The most common feeding structures that are used in microstrip patch antennas are:

- Coaxial Feed/Probe Coupling Feed
- Microstrip (Coplanar) Feed
- Proximity Coupled Microstrip Feed
- Aperture Coupled Microstrip Feed
- Coplanar Waveguide Feed

4.1 Importance of Feeding Structures

One of the most important factors in antenna design is efficient power transfer between radiator and input power structure. However, bending, junctions, transitions and terminations decrease the matching level. If the antenna feeding is not matched, reflection losses and spurious radiation increase. Due to the

undesired distribution of radiated power, side lobe and cross polarization levels also increase [6].

Another importance of feeding methods is in antenna arrays. In antenna arrays, different amplitude and phase requirements can easily be met by using appropriate feeding method. Basically, two types of feeding structures are used in antenna arrays. The first one is called parallel or corporate feed, in which the power enters from a single port and is distributed to multiple ports to supply the required amplitude and phase to the individual radiating elements. The second one is called series feed. This structure is based on a continuous transmission line from which small proportion of energy is coupled into the radiating elements by various means [3, 4]. By applying the appropriate coupling mechanism, equal and/or unequal power division can be achieved.

4.2 Coaxial Feed/Probe Coupling Feed

One of the common feeding methods is coupling of power through a probe. The most known advantage of this feeding is that the feed line is behind the radiating surface which prevents unwanted radiation from the probe lines. The feed location determines the input impedance Z_{in} which determines the impedance matching condition. Although the feeding structure is very simple, probe feed has several disadvantages. Because it needs several solder joints, the fabrication is difficult and should be done carefully. For thicker substrate longer probe should be used. However, longer probe causes increase in spurious radiation from the probe, surface wave power and feed inductance [3, 4].

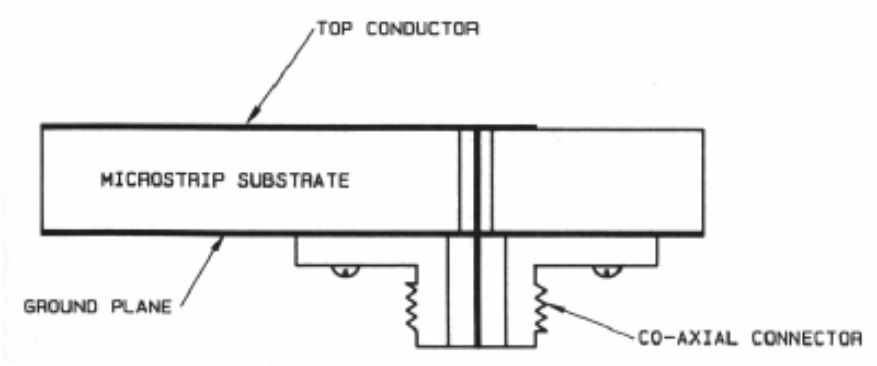

Figure 4-1: Buried Coaxial Line Feed [6]

There are basically two types of probe feed; buried coaxial line feed and panel launch coax line feed. The inner conductor of the former one passes through the substrate and soldered to radiating element. This structure is very simple; however, drilling via through the substrate and soldering the probe to the patch require careful handling. The inner connector of the panel launch coax line feed is soldered over microstrip line horizontally [3, 4, and 6]. The fabrication process is very practical in this case. The coax connector can easily be soldered to the substrate. In both structures the inductive characteristics of feed may increase due to physical discontinuities. This problem can be reduced by including a capacitive element in series.

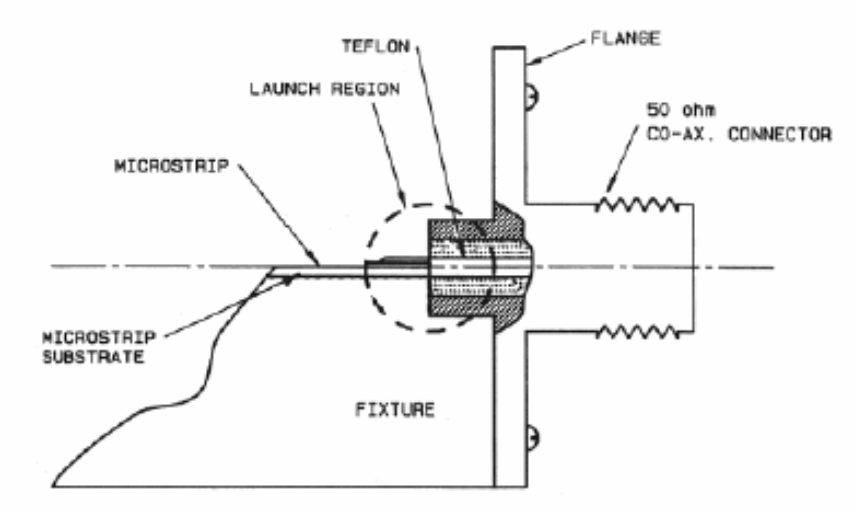

Figure 4-2: Panel Launch Coax Line Feed [6]

4.3 Microstrip (Coplanar) Feed

Another feeding method that transfers microwave power to the antenna elements is microstrip feed. The microstrip feed is easy to fabricate. This structure seems to be a natural choice, because the radiating patch can be considered as extension of microstrip feed line [3, 4, and 6]. The coplanar coupling is divided into two structures. One of them is direct coupled which the microstrip line is directly connected to the radiating element. The other one is gap coupled feed which requires a narrow gap between the radiating patch and microstrip line. Both structures have some limitations in design steps.

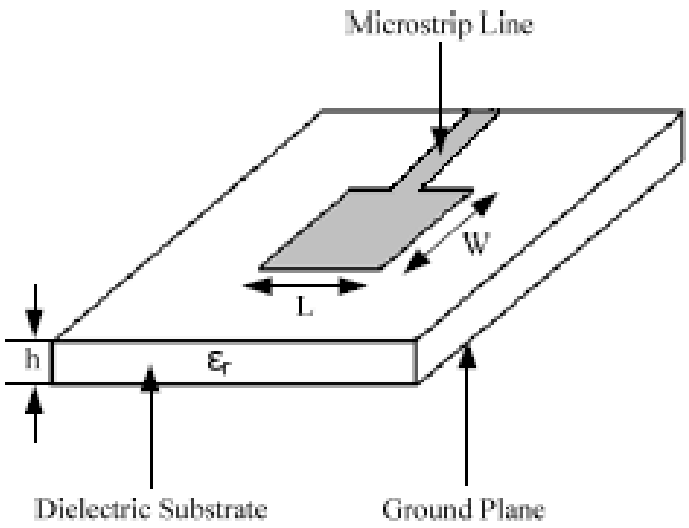

Figure 4-3: Microstrip (Coplanar) Feed [6]

The input impedance of the patch is much higher than the 50 ohm feed line. To connect the patch to the feeding line, some matching circuit should be used. However, these matching circuits give rise to undesired radiation. Moreover, these circuits are not usable in antenna arrays because they need more physical space on the substrate.

Because the feeding line is on the same plane with the radiating element, some power will also radiate from the line which deteriorates the radiation pattern of the patch. Moreover, the connection portion of the patch does not radiate, and this reduces the radiation. Gap coupled feeding structure (Figure 4-4) improves the radiation efficiency. Narrow gap width achieves efficient power transfer; however, the open end of the microstrip line also increases the spurious radiation.

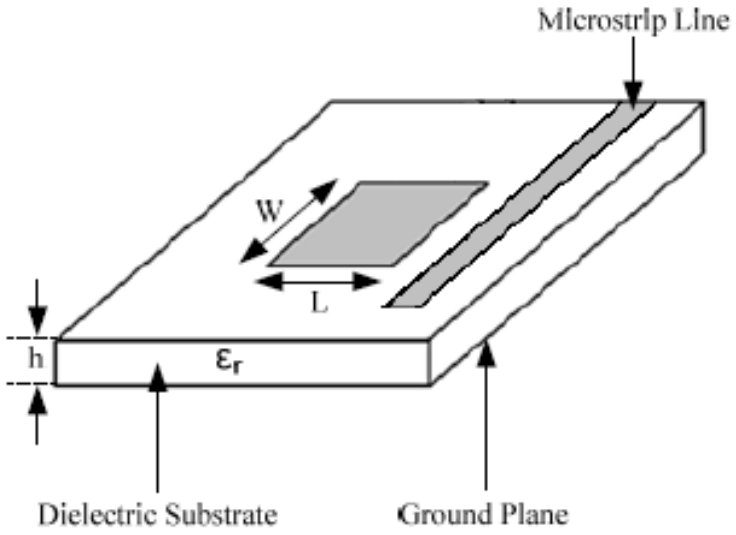

Figure 4-4: Gap Coupled Feed [3]

4.4 Proximity Coupled Microstrip Feed

This structure is based on gap coupled feeding method; however, in this structure, the microstrip line is on a different dielectric medium. Because the line is below the radiating surface, low spurious radiation will occur. The width of the line determines the input impedance. The open end of the line can be terminated by a stub and with appropriate design of the stubs the bandwidth can be increased. The disadvantages of this method are that the design and fabrication process are difficult. After the fabrication, the different dielectric layers should be aligned very carefully [3, 6].

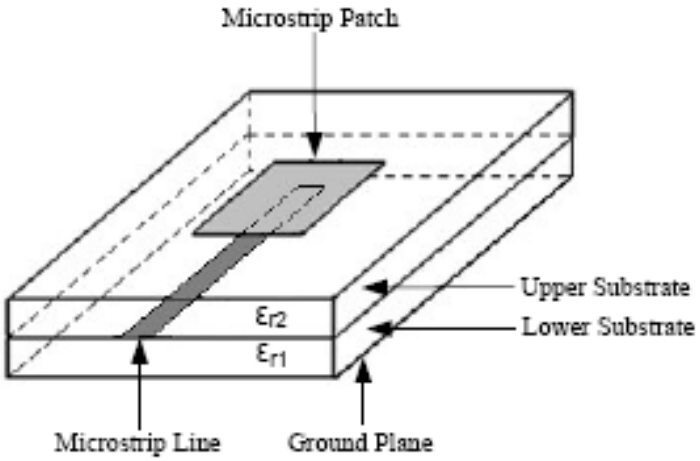

Figure 4-5: Proximity Coupled Microstrip Feed [3]

4.5 Aperture Coupled Microstrip Feed

Aperture Coupled feeding structure resembles the proximity coupling feed. The feed line passes below the radiating surface and the power enters to the radiating element by electromagnetic coupling through an aperture. The main improvement of this structure is that a ground plane exists between the two dielectric substrates. The ground plane does not permit spurious radiation from feed line and improves radiation purity.

The aperture should be placed on center symmetrically to transfer the maximum power. The matching conditions are met by adjusting the shape and size of the slot. The shape can be either circle or rectangle. Because matching condition depends on size and alignment of the different layers, the manufacturing process should be done carefully. To conclude, aperture coupling is very efficient way of exciting the patch antennas except for the drawback of difficulty on design and fabrication process.

4.6 Coplanar Waveguide Feed

Coplanar Waveguide Feed mostly resembles the aperture coupling. The coplanar wave guide is etched in the ground plane and coupling is accomplished via a slot as seen in Figure 4-5.

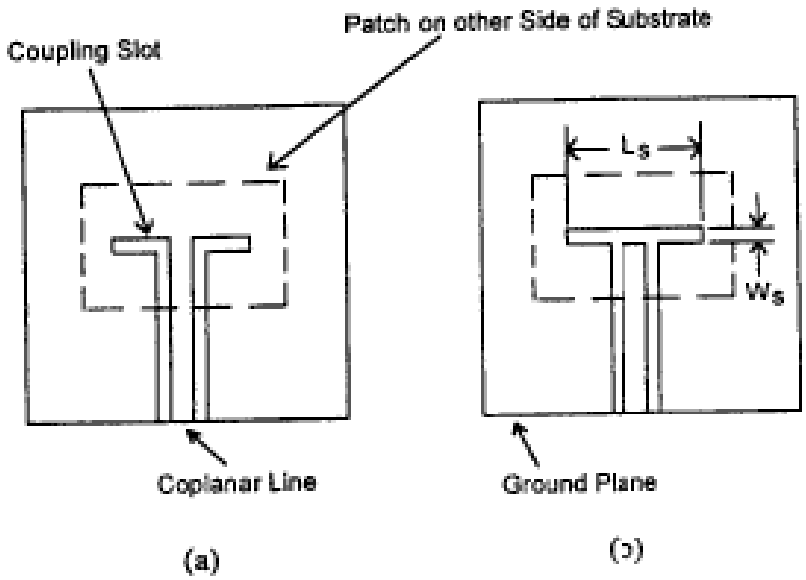

Figure 4-6: Coplanar Waveguide Feed Structures [4]

There are several possible structures of coplanar wave guide (CPW) feed. In Figure 4-5 (a), the center conductor of the CPW divides the coupling slot into two. In second structure, the CPW is transformed into slot of length L_s. The main advantage of these structures is seen on antenna arrays. The mutual coupling between adjacent lines is minimal and radiation from the feed structures is negligible [6].

4.7 Design considerations and decisions on Feeding Methods

The CDAR antenna is decided to include one coaxial connector at input port. In the laboratory, the antenna has to be connected to the test setup by a coaxial connector. There are two alternatives for coaxial feed; buried coaxial line feed and panel launch coaxial line feed. In CDAR antenna, buried coaxial line feed is used. The latter is not suitable for the prototype CDAR antenna, because there is no mechanical cover around the antenna and the panel launch connector could not be soldered or screwed to the system.

On the rest of the antenna system, after the power is divided into two, the power is transferred to the radiating patches by probe coupling. Small via holes are drilled on the lines of the power divider circuit and the patch surfaces. The via holes between the arms of the power divider circuit and the patches are connected by very thin wires. As mentioned in probe coupling section, this technique may have the drawback of spurious radiation or reflection. However, because the via heights are not comparable with the wavelength of the resonant frequency, these drawbacks are acceptable and it is not expected to deteriorate the antenna characteristics much.

CHAPTER 5

POWER DIVIDER and COUPLER DESIGN TECHNIQUES

Power dividers and couplers are needed in feeding structures of an antenna in various ways. They mostly are used in antenna arrays to meet the desired amplitude and phase requirements of each individual radiating element. Another usage of power dividers and couplers in feeding systems is in circular polarized antennas. As Huang mentioned, two orthogonal feeding excited with 90° phase difference satisfy circular polarization [3, 4, and 5]. In this chapter, various equal-unequal power dividers and couplers are investigated by considering their design approach. The advantages and disadvantages of these microwave circuits and design considerations are also discussed. The power division method used in CDAR antenna and its calculated design parameters is studied in chapter 6.

5.1 Wilkinson Power Divider

The Wilkinson Power Divider is the basic and one of the easiest ways of dividing the power equally/unequally. Wilkinson Power Divider is a lossy three port network and it has a property of being lossless when the output ports are matched. In addition, the isolation between output ports are can be achieved easily. However, due to the reflection from the input port and lossy transmission lines, some power is dissipated [7, 8].

In two port Wilkinson Power Divider, when the signal enters from port one, it splits the power into two equal amplitude and phase out signals at the second and the third ports. $2Z_0$ resistor accomplishes isolation between ports two and three. Because same potential exists at port two and port three, no current flows over isolation resistor. To satisfy the matching condition, the combined impedance of

output ports should be Z_0. Then the impedance values of quarterwave lines at the output ports must be equal to $\sqrt{2}Z_0$.

By Wilkinson Power Divider, unequal power split could be possible. This divider circuit is a two way Wilkinson Power Divider. The basic idea of unequal split is that dividing the power at quarterwave section on different impedance values; then, in the second section of quarterwave arms, transform the arm impedances back to Z_0. By this structure, the divider resembles 2-stage equal Wilkinson Power Divider. The expressions for quarterwave arm impedances are:

$$Z_{0A} = Z_0 * \left(\left(\frac{P_A}{P_B} \right)^{-1.5} + \left(\frac{P_A}{P_B} \right)^{-0.5} \right)^{0.5}$$

$$Z_{0B} = Z_0 * \left(1 + \frac{P_A}{P_B} \right)^{0.5} * \left(\frac{P_A}{P_B} \right)^{0.25}$$

$$Z_{0C} = Z_0 * \left(\frac{P_A}{P_B} \right)^{-0.25}$$

$$Z_{0D} = Z_0 * \left(\frac{P_A}{P_B} \right)^{0.25}$$

$$R_w = Z_0 * \left(\left(\frac{P_A}{P_B} \right)^{0.5} + \left(\frac{P_A}{P_B} \right)^{-0.5} \right)$$

where $\frac{P_A}{P_B}$ is the power division ratio in dB.

Figure 5-1 shows the basic structure, line impedances and isolation resistors of unequal split two-way Wilkinson Power Divider

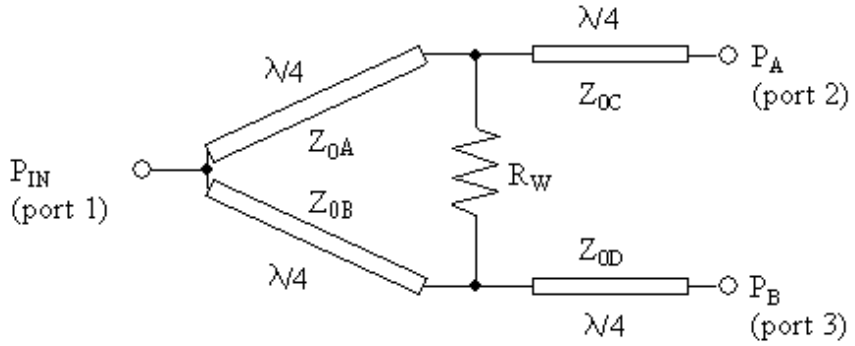

Figure 5-1: Unequal Split Wilkinson Power Divider [10]

In two-way unequal Wilkinson Power Divider, when the power division ratio increases, the impedance values start to differ from each other. This implies that one arm of the divider will be very thick; while the other one will be very thin. This is usually impractical to implement in manufacturing process.

5.2 Parallel Coupled Lines

For planar transmission lines (strip, microstrip etc.), parallel coupled transmission lines are frequently used in power division. Coupling occurs when two transmission lines are close enough in proximity. So the energy from one line passes to other line.

The basic, single section microstrip parallel coupled line is shown in Figure 5-2. The design of the coupler can be formulated by using even and odd mode impedances. The following equations are useful to find the Z_{0e} (even mode impedance) and Z_{0o} (odd mode impedance).

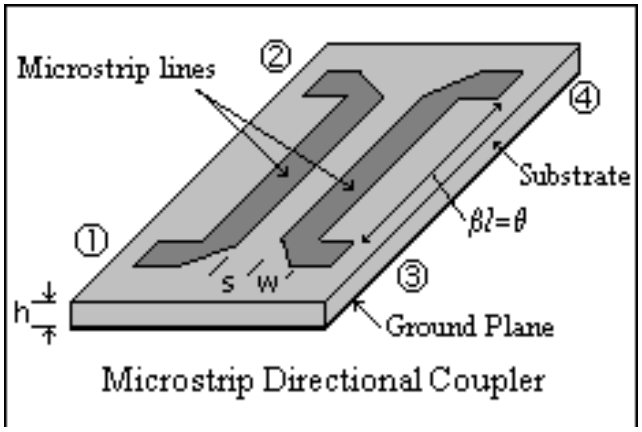

Figure 5-2: Line Coupled Directional Coupler [10]

Firstly, the coupling ratio "C" is selected. Then Z_{0e} and Z_{0o} will be calculated by using the following expressions:

$$Z_{0e} = Z_0 * \sqrt{\frac{1+C}{1-C}}$$

$$Z_{0o} = Z_0 * \sqrt{\frac{1-C}{1+C}}$$

where

$Z_0^2 = Z_{0e} * Z_{0o}$ is satisfied.

Secondly, by using the equations of shape ratio ω / h and spacing ratio s / h (where ω is the width of the lines, h is the thickness of the substrate, s is the spacing between the lines,) [6, 7 and 8], the desired line width and line length can easily be calculated.

Parallel coupled line is very common in literature; however, there are some disadvantages. The spacing between coupled lines is very critical. In some cases, the spacing will be very small and the production accuracy is not enough, so this makes the technique impractical to implement most cases.

5.3 Branchline Couplers

The branchline couplers are the simplest quadrature hybrids which divide the power equally/unequally by 90° phase shift. The easy production procedure comes from the entirely planar design.

Figure 5-3 shows the basic single box branchline coupler. This is also a four port network as other couplers discussed in this section. Each transmission line is quarter wave line to give higher bandwidth. 3/4, 5/4, 7/4 wavelength could be used on each line; however, this leads to decrease in bandwidth [3, 9, 10].

A basic 3 dB quadrature (90° phase shift) branchline coupler can be seen below. Port one is input and port four is isolated. Because port three has the longest path, it has the most negative phase difference.

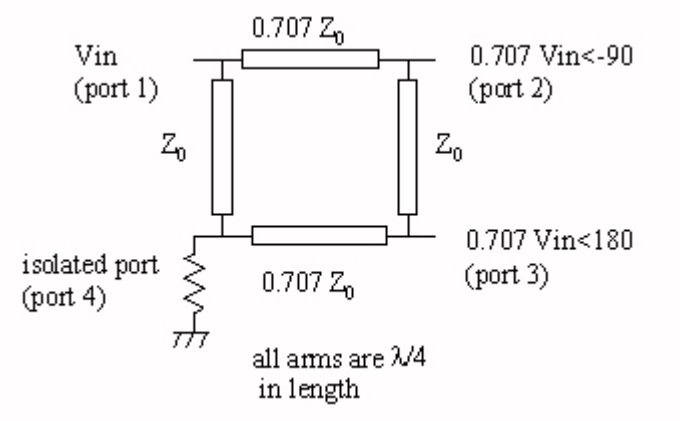

Figure 5-3: Single Box Branchline Coupler [11]

When the impedance values of opposite arms are varied, the coupler splits the power unequally. The phase difference will be same, because length of the arms are still quarter wave length.

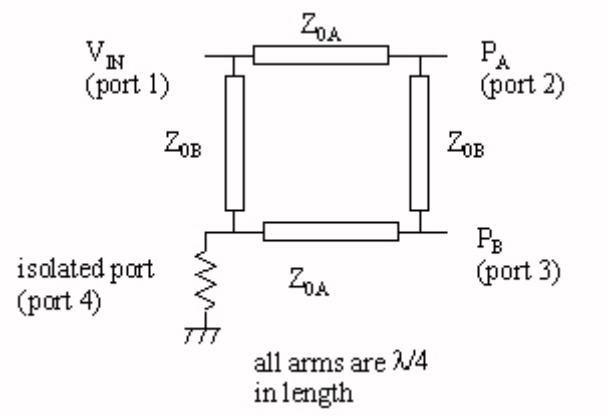

Figure 5-4: Unequal Power Split Branchline Coupler [12]

The following expressions give the relations between the coupling ratio "$C = \frac{P_A}{P_B}$" and impedance values.

$$Z_{0A} = Z_0 * \left(\frac{\frac{P_A}{P_B}}{1 + \frac{P_A}{P_B}} \right)^{0.5}$$

$$Z_{0B} = Z_0 * \left(\frac{P_A}{P_B} \right)^{0.5}$$

where $\frac{P_A}{P_B}$ is the coupling ratio in dB.

One can see the relation between impedance values of arms and coupling ratio in dB in Figure 5-5.

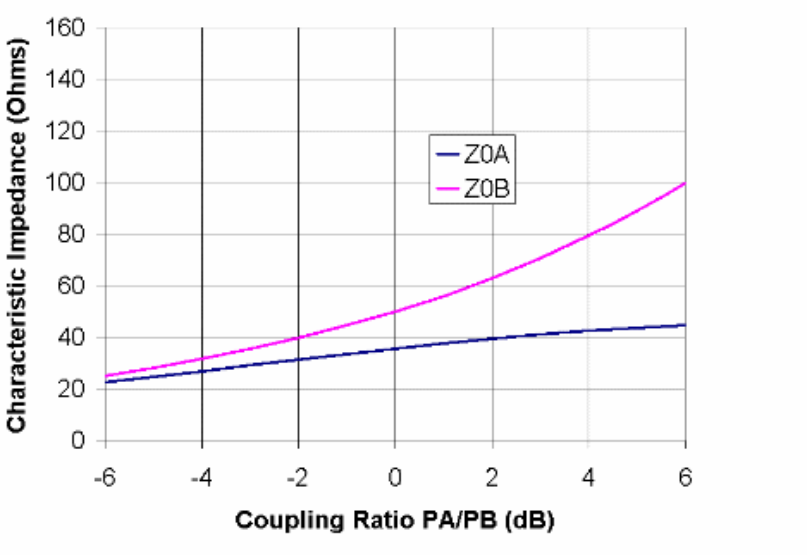

Figure 5-5: Coupling Ratio vs. Impedance Values of Z_{0A} and Z_{0B} [12]

As the coupling ratio increases, the impedance difference between Z_{0A} and Z_{0B} also increases. Due to this relation, if the coupling ratio is big, one of the arms will be very thick; while the other one will be very thin. The impedance values are impractical to implement in practice, for the coupling ratio above 6 or 7 dB. To sum up, up to 6 dB coupling ratio, the branchline coupler is used practically on coplanar surfaces, however after this point; the implementation will be a problem.

5.4 Broadside coupled line

Broadside coupler can be considered as a type of parallel line coupled directional coupler. The difference from parallel line coupled one is that the space between the lines is not coplanar. The arms are on different planes and between the lines, there is dielectric substrate layer. The lines could have also offset in their position which provides higher coupling ratio than parallel line coupled directional couplers.

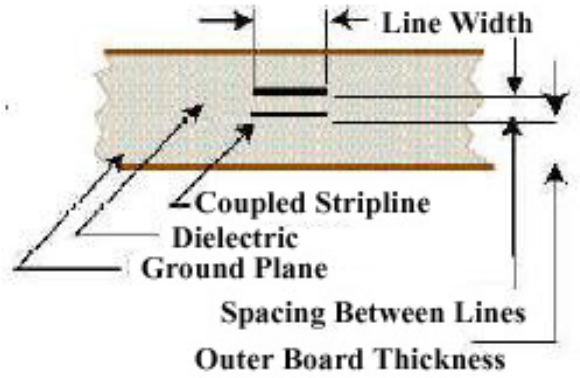

Figure 5-6: Broadside Coupler [8]

Certain relations among Z_0 (characteristic impedance), C (coupling ratio in dB), b (substrate thickness), s (line spacing), ω (line width) are given in the following expressions. As seen from the Figure 5-6, symbols "s" and "ω" represents the ratio of line spacing and line width to the total ground plane spacing. The total ground plane spacing is the sum of the thickness of three boards.

"C" is the coupling ratio in dB.

$$V = e^{\frac{C}{-8.68589}} \qquad \text{where} \quad -8.68589 = -\frac{20}{\log_e(10)}$$

$$\frac{Z_{0e}}{Z_{0o}} = \frac{1+V}{1-V} \qquad \text{which satisfies } Z_{0e} * Z_{0o} = Z_0^2$$

$$Z_{0e} = \frac{188.3}{\sqrt{\varepsilon_r}} \frac{K(k')}{K(k)} \qquad \text{where } K(k) \text{ is the elliptic integral equation to the first kind}$$

[12].

$$k' = \sqrt{1 - k^2} \qquad \text{and} \qquad Z_{0o} = \frac{296.1 * s}{\sqrt{\varepsilon_r} * \tanh^{-1}(k)}$$

After finding Z_{0e} and Z_{0o} from the solution of the elliptic integral equation to the first kind, one can write the following expressions [11].

$$w = \frac{2}{\pi}\tanh^{-1}(R) - s * \tanh^{-1}(\frac{R}{k})$$

$$R = \sqrt{\frac{k - s}{\frac{1}{k} - s}}$$

Broadside couplers are one of the most practical couplers for stripline structures. Especially for high coupling ratio, broadside couplers are easy to implement and fabricate. However, because the offset between the arms is also effective in coupling, the alignment should be very accurate. This defect can be eliminated at the design stage by using appropriate substrate and choosing appropriate substrate thickness.

5.5 Design considerations for Power Dividers

As discussed in this chapter, all power dividers and couplers have some advantages and disadvantages. To choose the appropriate one, one should state the requirements of his design well. For example, for 3 dB power division, Wilkinson Power Divider may be the easiest design; on the other hand, it could not be used in broadband applications.

For broadband applications, line coupled and branchline couplers work well, however, one should consider the production processes.

In this thesis study, the CDAR antenna needs 10 dB coupling ratio with in phase output. Because unequal power division and high coupling ratio is needed, the best fitted and practical method is Broadside Coupler. The other structures all have some implementation and manufacturing problems.

CHAPTER 6

CIRCULAR DISK ANNULAR RING (CDAR) MICROSTRIP PATCH ANTENNA DESIGN

After discussing the microstrip patch antennas, circular polarization techniques, feeding structures and couplers, in this chapter, the design procedure of CDAR antenna is discussed. The design step starts by substrate selection. Afterwards, singly-fed circularly polarized circular disk antenna is investigated. Thirdly, singly-fed circularly polarized annular ring antenna element is studied. The design parameters of single radiator elements are calculated for the resonant frequency 8.2 GHz. The simulation results of circular disk antenna and annular ring at the given resonant frequency are also included. Then, the next topic deals with the super position of the single antenna elements. After super position, the resonant frequency is changed due to coupling between the patches; therefore the radius of patches should be optimized for resonant frequency. The optimization of patch radii is also studied in this topic. Finally, the structure of the complete CDAR antenna and the Ansoft Ensemble 8.0 simulation results are given at the end of this chapter.

The main idea of the CDAR antenna is super position of a Circular Disk patch antenna in dominant TM_{11} mode and an Annular Ring patch antenna in TM_{12} mode. The radiation pattern of Circular Disk patch in TM_{11} mode (Figure 6-1(a)) is superposed with the radiation pattern of Annular Ring patch in TM_{12} mode (Figure 6-1(b)). After the super position of the two radiation patterns by applying appropriate amplitude and phase constants, the desired pattern is accomplished (Figure 6-2).

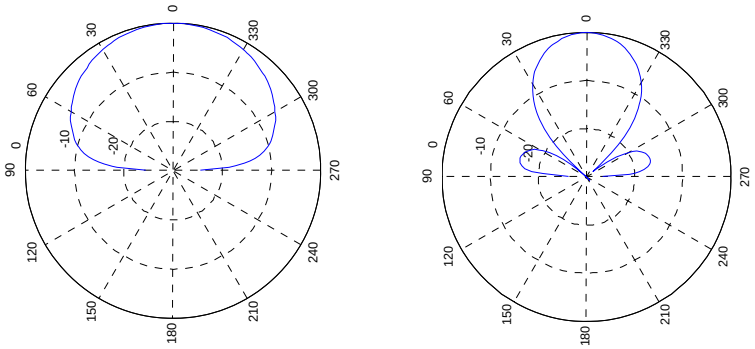

(a) (b)

Figure 6-1: Normalized Radiation Patterns of (a) Circular Disk Antenna and (b) Annular Ring Antenna

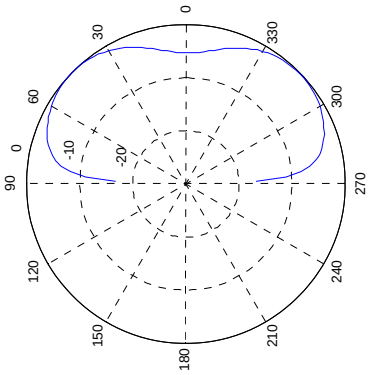

Figure 6-2: Normalized Radiation Pattern of CDAR Antenna

6.1 Dielectric Substrate of CDAR Antenna

As described in Chapter Two, microstrip patch antenna should have a thicker substrate and lower permittivity to increase the radiation efficiency. However, the substrate thickness should not exceed $0.1\lambda_0$ since otherwise surface waves may

be excited [6]. The free space wavelength of the design frequency is $\lambda_0 \cong 36$ mm which means that the substrate thickness should be below 3.6 mm.

Finally, the product of Rogers Corporation, RT/duroid® 5880 type dielectric substrate [7] is chosen. The product has low dielectric constant ($\varepsilon_r = 2.2$) and other product specifications are suitable for CDAR antenna [13]. The antenna is printed on a dielectric substrate of thickness 1.57 mm while dielectric layers of thicknesses 0.51 mm and 0.127 mm are used for feed layers.

6.2 Singly-fed Circularly Polarized Circular Disk Antenna Design

The circular disk antenna design parameters such as radius of the patch, feeding point location and perturbation segments area (used for singly-fed circular polarization) can easily be calculated from the expressions discussed in chapter two and three. However, the antenna design parameters are affected from the substrate thickness and perturbation segments. In this study, these parameters are firstly calculated analytically and then optimized by using simulation program.

The first basic parameter is the radius of the circular disk antenna which determines the resonant frequency. The radius of the patch is calculated as:

$$r = \frac{\lambda_{11} c}{2\pi f \sqrt{\varepsilon_r}}$$

where:

$\lambda_{11} = 1.84118$ is the first root of the derivative of the Bessel Function of order 1,

$c = 2.98 * 10^8$ is the speed of light in m/s

$f = 8.2 * 10^9$ is the resonant frequency in Hz.

$\varepsilon_r = 2.2$ is the dielectric constant of RO 5580 Duroid substrate.

With these parameters, the radius of the disk is calculated as 7.18 mm. The effective radius will be slightly different than the calculated one. By using the following expression stated in Chapter Two, the more accurate effective radius can easily be found:

$$r_e = r\left\{1 + \frac{2h}{\pi r \varepsilon_r}\left(\ln\frac{\pi r}{2h} + 1.7726\right)\right\}^{1/2}$$

where

r_e is the effective radius of the patch

$r = 7.18$ mm is the calculated radius of the patch

$h = 1.57$ mm is the substrate thickness.

The effective radius of the Circular Disk Antenna is calculated as 7.98 mm. However, after implementation of singly-fed circular polarization method, the patch radius needs to be optimized. After the simulations in Ansoft Ensemble 8.0 program, the optimized disk radius is 6.25 mm.

Secondly, the feed location is another important design parameter which satisfies the matching condition. To determine the feed location analytically, the following expression can be used.

$$R_{in} = R_r \frac{J_1^2(k_{11}\rho_0)}{J_1^2(k_{11}r)}$$

where

$R_{in} = 50\Omega$ is the desired input impedance of antenna

R_r is the radiation resistance of the antenna [3,4]

$k_{11} * r = 1.84118$ is the first root of the derivative of the Bessel Function of order 1.

Then, the distance of the feeding point from the antenna center is found as $\rho_0 = 1.26$ mm.

The angular position of the feeding point is not important, because there is no preferred axis for circular disk patch. However the feeding point should be optimized after perturbation method used for circular polarization. The feeding point is selected as $\rho_0 = 1.5$ mm after considering the simulation results at resonant frequency of 8.2 GHz.

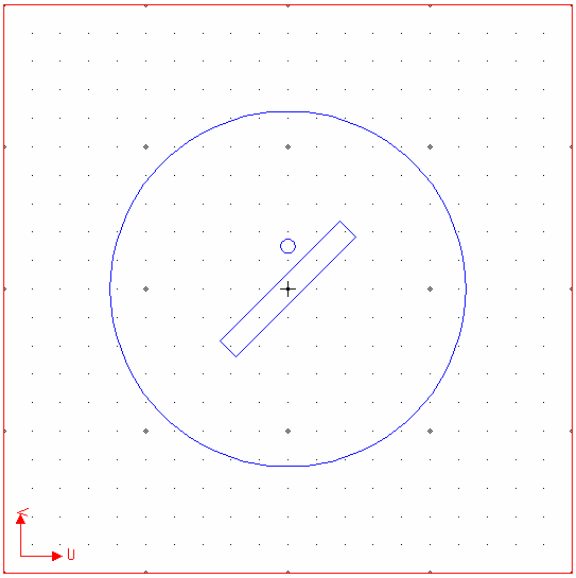

Figure 6-3: Structure of Singly-fed Circularly Polarized Circular Disk Antenna

Lastly, the circular polarization is achieved by a perturbation segment. The perturbed area in the middle of the disk (Figure 6-3) creates two orthogonal modes in equal amplitude and 90° phase difference. These two orthogonal modes causes the patch to radiate circularly polarized waves. The area of the perturbation segment is calculated as:

$$\left|\frac{\Delta S}{S}\right| = \frac{1}{x_{11} Q_0}$$

ΔS is the total perturbation area

S is the total patch area

$x_{11} = 1.84118$ which is the first root of derivative of Bessel function of order 1

Q_0 is the unloaded quality factor defined in chapter three.

The perturbation area is calculated as $\Delta S = 4.4$ mm^2. However, the perturbation segment changes the effective radius of the disk and the location of the feeding point. These parameters are optimized by simulations. Figure 6-4 and 6-5 show the S_{11} and Radiation Pattern of the circularly polarized Circular Disk Antenna designed at the center frequency of 8.2 GHz.

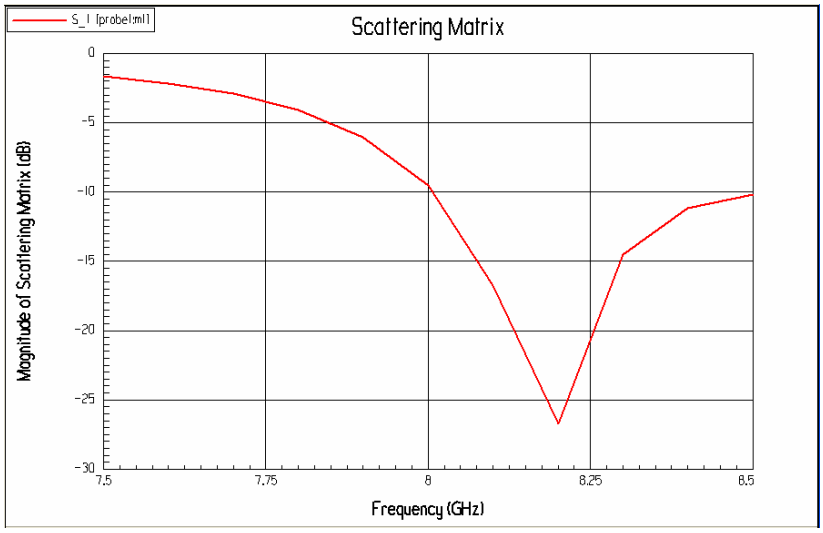

Figure 6-4: S_{11} Figure of Singly-fed Circularly Polarized Circular Disk Antenna

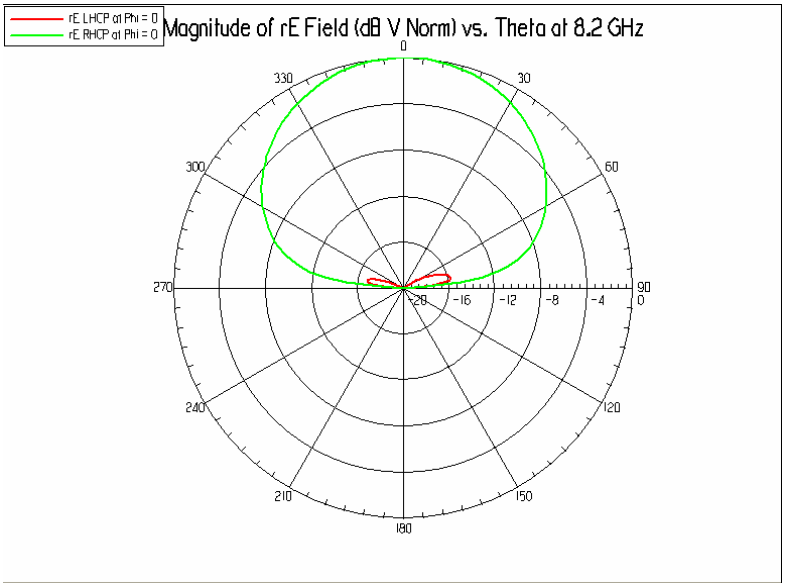

Figure 6-5: Radiation Pattern of Singly-fed Circularly Polarized Circular Disk Antenna

6.3 Singly-fed Circularly Polarized Annular Ring Antenna Design

The dominant mode TM_{11} for Annular Ring antenna gives a pattern similar to the one in Circular Disk antenna. To achieve the desired radiation pattern, we need to excite the ring antenna in a higher order mode. The best fitted higher order mode is selected as TM_{12} for annular ring patch.

From the expressions given in chapter two, the inner radius "a" and the outer radius "b" of annular ring antenna can easily be calculated. However, b/a ratio should be selected to find the root of characteristic equation χ_{12}. Considering the simulation results, to eliminate the coupling problem between the disk and the ring radiators, the inner radius of the ring antenna should be nearly 10% greater than the radius of the disk antenna. To satisfy this requirement, the b/a ratio is selected as $b/a = 2.5$. Then, the root of the characteristic equation is found to be $\chi_{12} = 2.2635$ and the inner radius of the ring is calculated as $a = 8.8$ mm. However, the substrate thickness and the perturbation segments affect the actual radius of the patch and change the resonant frequency. After the simulations, the effective inner and outer radii of the ring are $a_e = 8.4$ mm and $b_e = 21$ mm.

The feed location is also an optimization problem. To satisfy a good matching condition, the feed location must be close to the inner radius. However, this location is also affected by perturbation segments as in circular disk case. Considering the polarization technique used in CDAR antenna, the ρ_0 is selected as $\rho_0 = 9.5\,\text{mm}$.

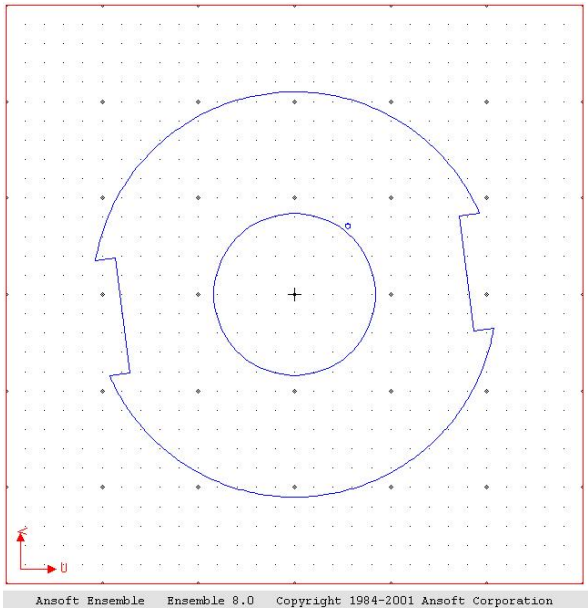

Figure 6-6: Structure of Singly-fed Circularly Polarized Annular Ring Antenna

The singly-fed circular polarization is accomplished by perturbation method as stated before. The perturbation segments are located on the outer radius of the patch to minimize the effect on circular disk radiation (Figure). These segments divide the excitation into two orthogonal modes in equal amplitude and 90° phase difference. These two orthogonal modes causes the patch to radiate circularly polarized waves. The perturbed area can be calculated by similar expression given in circular disk antenna. The total perturbation area is found as $\Delta S = 52.8$ mm^2. However, as in the circular disk antenna case, the perturbation segments change the effective radius of the ring patch and the location of the feeding point. These parameters are optimized by simulations. Figures 6-7 and 6-8 show the S_{11} and Radiation Pattern of the circularly polarized Annular Ring Antenna designed at the center frequency of 8.2 GHz.

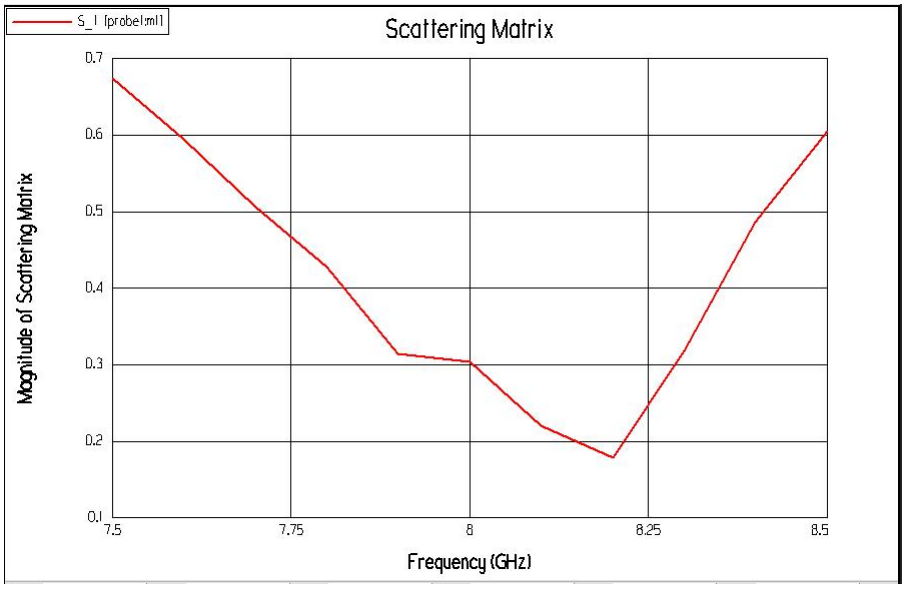

Figure 6-7: S_{11} Figure of Singly-fed Circularly Polarized Annular Ring Antenna

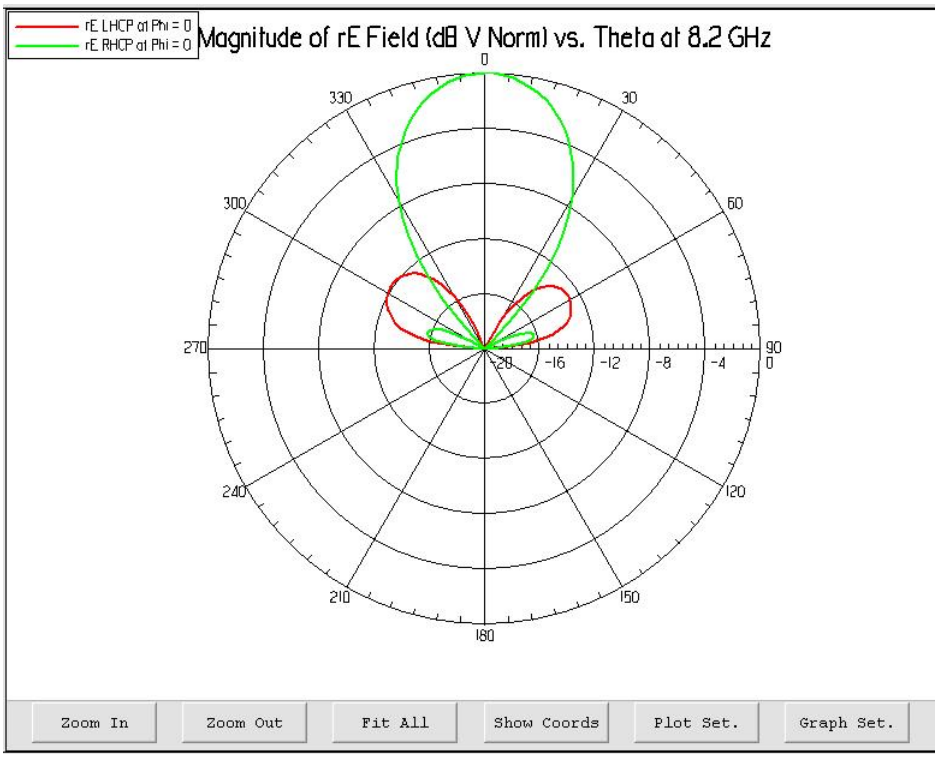

Figure 6-8: Radiation Pattern of Singly-fed Circularly Polarized Annular Ring Antenna

6.4 Super Position of Circular Disk and Annular Disk Antenna

As stated before, the CDAR antenna is a combination of a Circular Disk and an Annular Ring patch antenna. The pattern data obtained from the simulation results of single antenna elements are superposed by the appropriate multiplication constants, and the resultant pattern data satisfies the desired radiation pattern. To find this result analytically, one can use the E_θ and E_ϕ field expressions given in Huang [5]. Huang claims that the four probe feed, excited by 0°, 90°, 180°, and 270° degree phase differences, gives circular polarized E_θ and E_ϕ field expressions.

The analytical expressions include four probe excitation by equal amplitude and 0°, 90°, 180°, and 270° phase differences. The general E_θ and E_ϕ field expressions of both disk and ring antennas are [5]:

$$E_\theta^t = E_\theta(\phi,\theta) + jE_\theta(\phi+\pi/2,\theta) - E_\theta(\phi+\pi,\theta) - jE_\theta(\phi+3\pi/4,\theta)$$

$$E_\phi^t = E_\phi(\phi,\theta) + jE_\phi(\phi,\theta+\pi/2) - E_\phi(\phi,\theta+\pi) - jE_\phi(\phi,\theta+3\pi/4)$$

For Circular Disk Antenna, E_θ and E_ϕ fields in TM_{11} mode are:

$$E_\theta(\theta,\phi) = \left[J_2(k_0 a\sin\theta) - J_0(k_0 a\sin\theta)\right]\cos(\phi)$$

$$E_\phi(\theta,\phi) = \left[J_2(k_0 a\sin\theta) + J_0(k_0 a\sin\theta)\right]x\cos(\theta)\sin(\phi)$$

For Annular Ring Antenna, E_θ and E_ϕ fields in TM_{12} mode is:

$$E_\theta(\theta,\phi) = \cos(\phi)\left[J_1^{'}(k_0 b\sin(\theta)) - \frac{J_1^{'}(k_{nm}b)}{J_1^{'}(k_{nm}c)}J_1^{'}(k_0 c\sin(\theta))\right]$$

$$E_{\phi}(\theta,\phi) = \cos(\theta)\sin(\phi)\left[\frac{J_1^{'}(k_0 b\sin(\theta))}{k_0 b\sin(\theta)} - \frac{J_1^{'}(k_{nm}b)}{J_1^{'}(k_{nm}c)}\frac{J_1^{'}(k_0 c\sin(\theta))}{k_0 c\sin(\theta)}\right]$$

where

a is the radius of Circular Disk Antenna

b is the inner radius of Annular Ring Antenna

c is the outer radius of Annular Ring Antenna

For super position, one can add the circularly polarized radiation fields of single antenna elements by a constant magnitude value β. Afterwards, the expression is differentiated with respect to θ and equated to zero. One can easily find the maxima and minima angles of θ by solving this equation. Then, after putting the θ values to radiation field expressions, the difference between the maxima and the minima angles is the value of the required difference at broadside angle. One can find the amplitude values of single antenna elements for the desired decrease level in power pattern. The following expressions show the process steps discussed in this paragraph.

1. Add the circularly polarized radiation field equations by amplitude constant β

$$E_{\theta}^{CDAR}(\theta,\phi) = E_{\theta}^{DISK}(\theta,\phi) + \beta * E_{\theta}^{RING}(\theta,\phi)$$

$$E_{\phi}^{CDAR}(\theta,\phi) = E_{\phi}^{DISK}(\theta,\phi) + \beta * E_{\phi}^{RING}(\theta,\phi)$$

where

$E_{\theta}^{CDAR}(\theta,\phi)$, $E_{\phi}^{CDAR}(\theta,\phi)$, $E_{\theta}^{DISK}(\theta,\phi)$, $E_{\phi}^{DISK}(\theta,\phi)$, $E_{\theta}^{RING}(\theta,\phi)$ and $E_{\phi}^{RING}(\theta,\phi)$ are the circularly polarized far field pattern equations given in chapter 3.

β is the amplitude constant

2. Then, differentiate the CDAR antenna field equation and equate the result to zero for finding maxima and minima points.

$$\frac{E_{\theta}^{CDAR}(\theta,\phi)}{\partial\theta} = 0$$

Then, two maxima and one minimum angle points can easily be found.

3. Put the maxima and minima angle values to the radiation field expression and subtract them. The difference is the value of the required difference at broadside angle. By solving the equation after equating it to the required power level, one can find the β value easily (Appendix 1).

Figure 6-9 shows the variation of Amplitude ratio of Ring antenna (β) versus Desired Power Ratio in dB. The radii are selected as the optimized ones that are used in simulation and fabrication. It can be seen from the figure, that the more ring antenna is excited, the more power at broadside angle will decrease. Actually, this formulation is not exact, since it does not include the mutual coupling and single-fed circular polarization effects. However, this result gives enough accuracy and very good perspective for how to excite the disk and ring antennas.

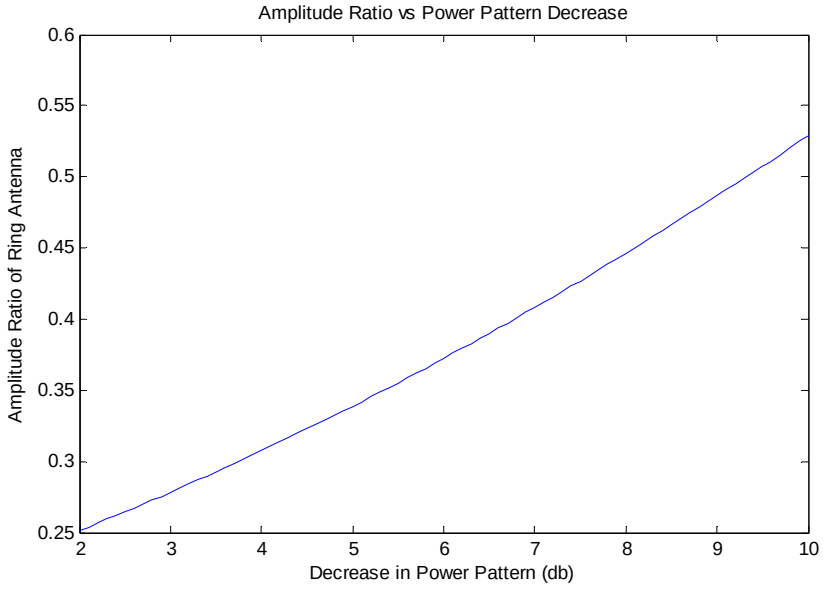

Figure 6-9: Amplitude Constant vs. Decrease Level in Power Pattern in dB

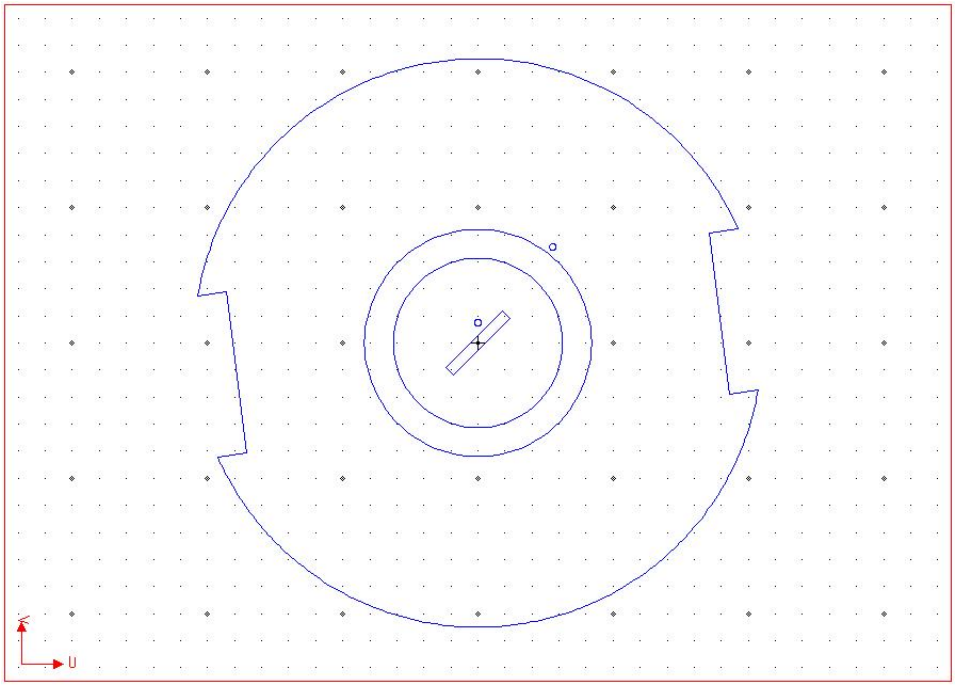

Figure 6-10: Structure of Two Probe Feed Circularly Polarized CDAR Antenna

Following figures show the simulation results of CDAR antenna exited from two probes. The disk patch is excited by amplitude constant of one, and the ring patch is excited by amplitude constant of 0.3. As seen from Figure 6-12, the ring patch excitation by amplitude of 0.3 satisfies nearly 3 dB power decrease at broadside angle.

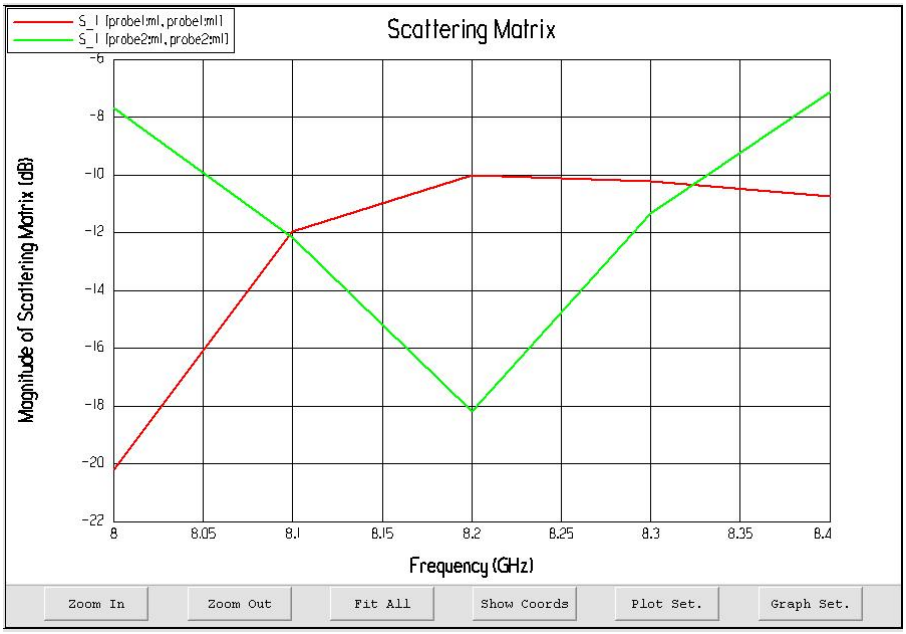

Figure 6-11: S_{11} and S_{22} Figure of Two Probe Feed Circularly Polarized CDAR Antenna

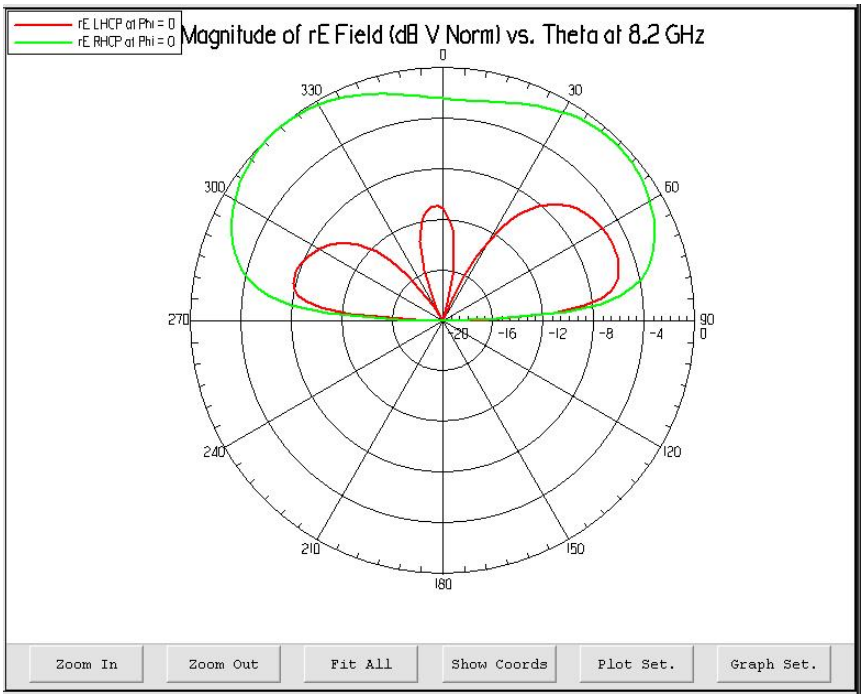

Figure 6-12: Radiation Pattern of Two Probe Feed Circularly Polarized CDAR Antenna

6.5 Feeding Structures of CDAR

Array antenna structure requires two or more excitation points. However, the power enters to the system from single input port. Then, in antenna arrays, designers should divide the power appropriately to the separate antenna elements.

The CDAR antenna needs two feeding points excited with amplitude constant of 1 for circular disk patch, and amplitude constant of 0.3 for annular ring patch in phase. This excitation satisfies 3 dB power difference between maxima and minima points in main lobe.

To excite the antenna by amplitude constants of 1 and 0.3, nearly 10 dB power division is required. To achieve the 10 dB power division, four different types of power divider and/or couplers are examined in this study. The 10 dB power divider and/or couplers studied in this thesis are:

- Wilkinson Unequal Power Divider
- Parallel Coupled Line
- Branchline Coupler
- Broadside Coupler

As discussed in chapter 5, all these microwave circuits have advantages and disadvantages. To select the appropriate one for the CDAR antenna, all the microwave circuits are designed for 10 dB power division and simulated in ADS 2004A simulation program. Rogers Corporation 0.51 mm RO5880 substrate is used in all the circuits. The designed circuits and the calculated design parameters are introduced below.

- **Wilkinson Unequal Power Divider**

Wilkinson power divider is one of the simplest ways of power split. It is also easy to manufacture. The output powers are in phase as desired in CDAR antenna. The following values are calculated by the expressions given in chapter 5. The impedance and line widths are:

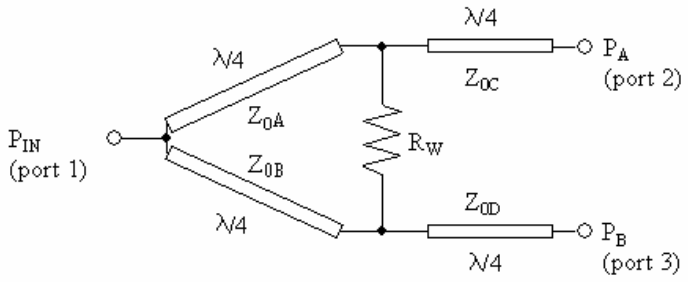

Figure 6-13: Unequal Split Power Divider

Rogers RO5880 Substrate Thickness: $h = 0.51$ mm

Rogers RO5880 Substrate Dielectric: $\varepsilon_r = 2.2$

$$C = 10db \Rightarrow \frac{P_A}{P_B} = 10$$

$$Z_{0A} = 50 * \left((10)^{-1.5} + (10)^{-0.5}\right)^{0.5} \cong 29.49\Omega \Rightarrow\Rightarrow\Rightarrow W_{0A} \cong 3.25mm$$

$$Z_{0B} = 50 * (10+1)^{0.5} * (10)^{0.25} \cong 294.89\Omega \Rightarrow\Rightarrow\Rightarrow W_{0A} \cong 0.0073mm$$

$$Z_{0C} = 50 * (10)^{-0.25} \cong 28.12\Omega \Rightarrow\Rightarrow\Rightarrow W_{0A} \cong 3.457mm$$

$$Z_{0C} = 50 * (10)^{0.25} \cong 88.91\Omega \Rightarrow\Rightarrow\Rightarrow W_{0A} \cong 0.585mm$$

$$R_W = 50 * \left((10)^{0.5} + (10)^{-0.5}\right) \cong 173.93\Omega$$

The calculated design parameters are hard to manufacture. The high impedance line is very thin; while the other one is very thick. Then, it is obvious that unequal Wilkinson power divider is hard to implement and not appropriate for CDAR feeding structure.

- **Parallel Coupled Line**

The design parameters of the Parallel Coupled Line are:

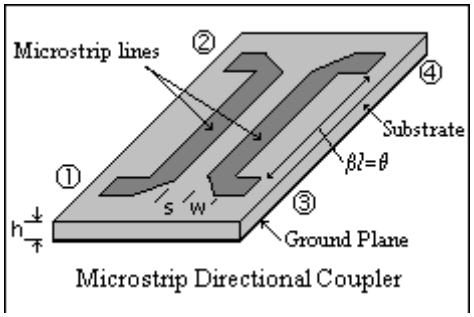

Figure 6-14: Parallel Coupled Line Structure

Rogers RO5880 Substrate Thickness: $h = 0.51$ mm

Rogers RO5880 Substrate Dielectric: $\varepsilon_r = 2.2$

$C = 10db \Rightarrow K = 0.316$

$$Z_{0e} = 50 * \sqrt{\frac{1+0.316}{1-0.316}} = 69.36\Omega$$

$$Z_{0o} = 50 * \sqrt{\frac{1-0.316}{1+0.316}} = 36.03\Omega$$

$w = 1.295mm$

$s = 0.057$mm

For high coupling ratio, the spacing between the parallel lines is very narrow and sensitive. The standard LPKF machines have 6 mil (0.15 mm) error margins. This error margin does not allow manufacturing of this microwave circuit on standard LPFK machines. To conclude, this microwave circuit is also not appropriate for the CDAR antenna.

- **Branchline Coupler**

The branchline couplers are widely used because of their simple production processes. However, after the coupling ratio reaches to 6-7 dB, the branchline couplers are impractical to be manufactured. This is due to the asymmetry on the line width. For the CDAR antenna design, design parameters for 10 dB branchline coupler are calculated as:

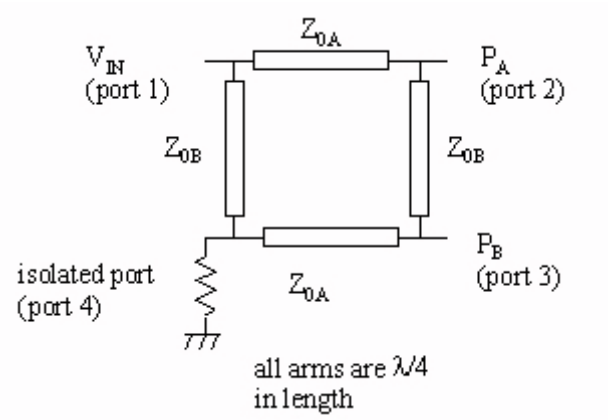

Figure 6-15: Unequal Split Branchline Coupler

Rogers RO5880 Substrate Thickness: $h = 0.51$ mm

Rogers RO5880 Substrate Dielectric: $\varepsilon_r = 2.2$

$$C = 10db \Rightarrow \frac{P_A}{P_B} = 10$$

$$Z_{0A} = 50 * \left(\frac{10}{1+10} \right)^{0.5} \cong 47.67\Omega \Rightarrow\Rightarrow\Rightarrow w = 1.689mm$$

$$Z_{0A} = 50 * (10)^{0.5} \cong 158.11\Omega \Rightarrow\Rightarrow\Rightarrow w = 0.131mm$$

- **Broadside Coupler**

Broadside couplers resemble to parallel coupled lines. Also the spacing between the lines is still critical for coupling ratio; however, in this case, the spacing is in the "z" axis and it is the thickness of dielectric substrate between the lines. So, the spacing does not affect and restrict the manufacturing process. To conclude, broadside couplers are one of the best selections for high coupling ratio problems. In CDAR feeding structure, broadside coupler is selected to be used for 10 dB power division.

The calculated values for 10 dB coupling ratio are:

Rogers RO5880 Substrate Thickness: $h = 0.51$ mm

Rogers RO5880 Substrate Dielectric: $\varepsilon_r = 2.2$

$C = 10db \Rightarrow K = 0.316$

$$Z_{0e} = 50 * \sqrt{\frac{1+0.316}{1-0.316}} = 69.36\Omega$$

$$Z_{0o} = 50 * \sqrt{\frac{1-0.316}{1+0.316}} = 36.03\Omega$$

$$w = 0.78mm$$

$$w_0 = 0.775mm$$

$$s = 0.127\text{mm}$$

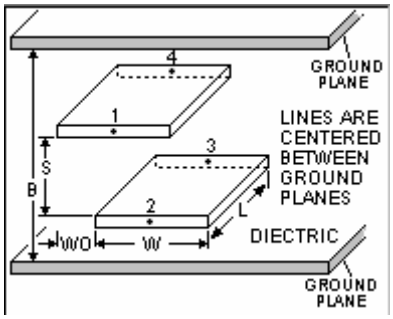

Figure 6-16: Broadside Coupler Structure

The broadside coupler designed for the CDAR antenna is simulated in ADS 2004A and also in Ansoft Ensemble 8.0 simulation programs. The circuit schematics and simulation results in ADS 2004A and Ensemble software are shown below.

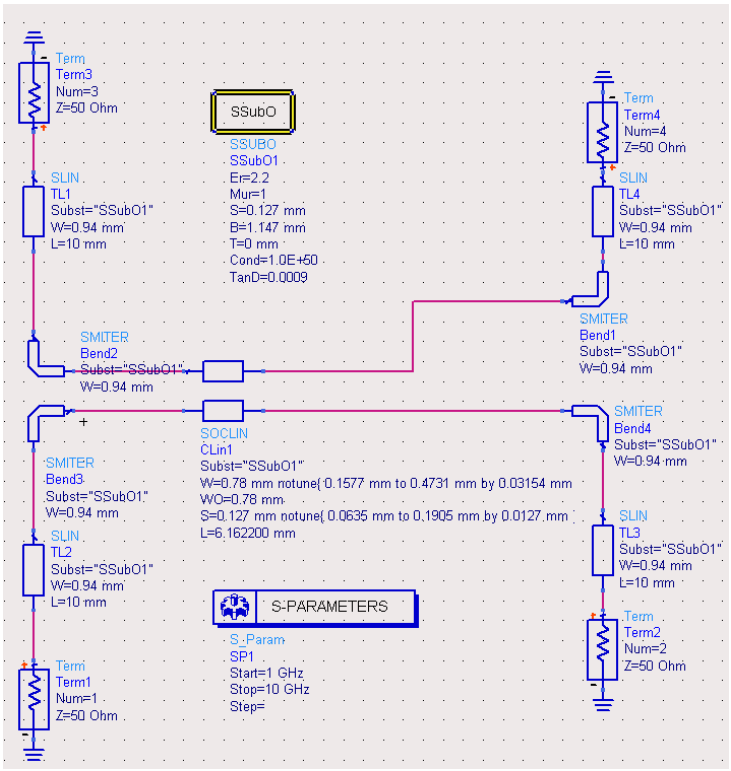

Figure 6-17: ADS Simulation Circuit Schematics of 10 dB Broadside Coupler

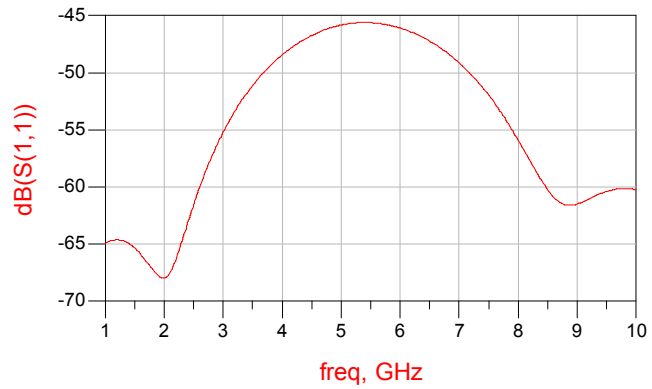

Figure 6-18: S_{11} (Reflection) vs. Frequency Simulation Result in ADS in dB scale

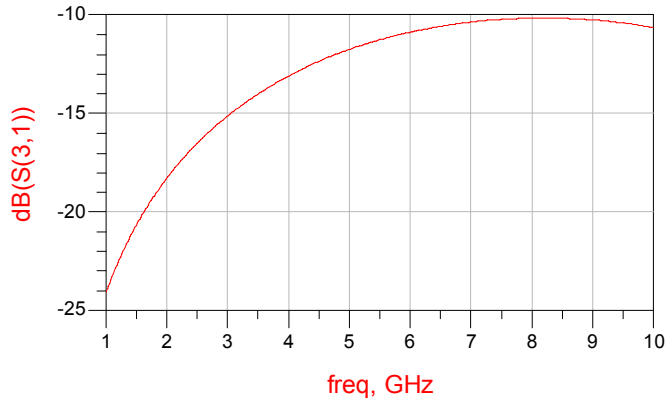

Figure 6-19: S_{31} (Coupled Port) vs. Frequency Simulation Result in ADS in dB scale

This structure is simulated in Ensemble Simulation software, and the S_{11} (Reflection) and S_{31} (Coupled Port) graphs at resonant frequency 8.2 GHz are given below:

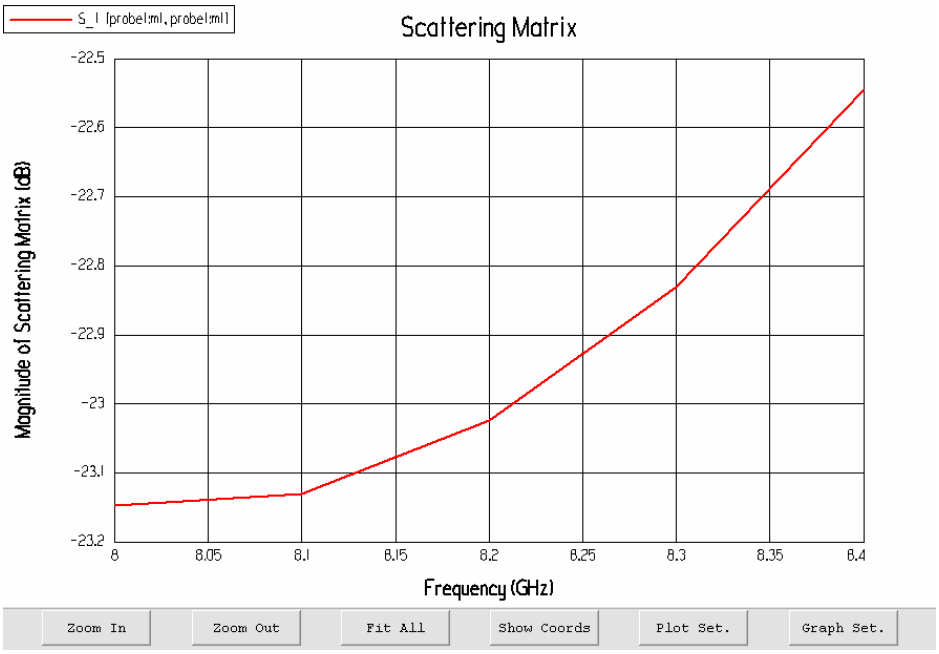

Figure 6-20: S_{11} (Reflection) vs. Frequency Simulation Result in Ensemble

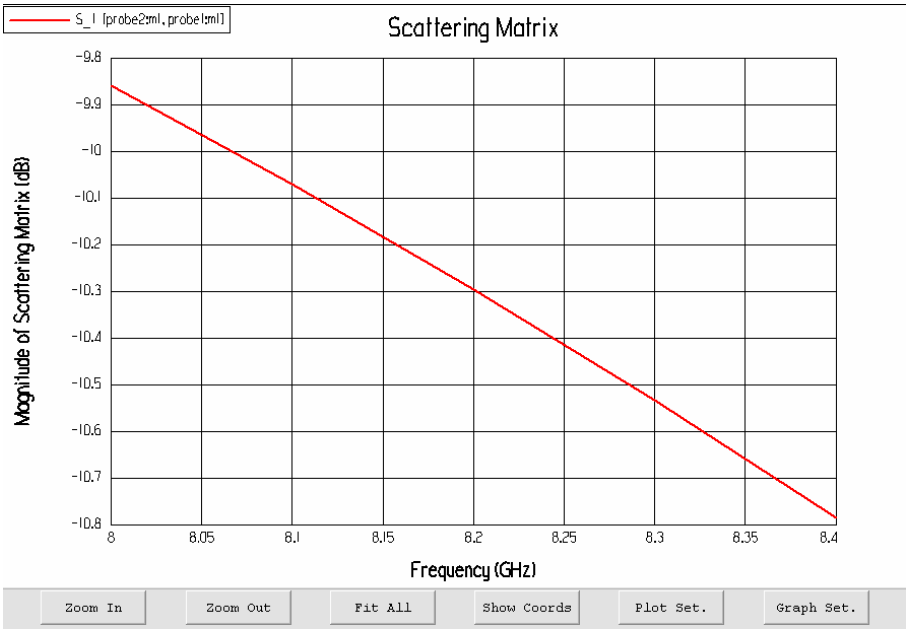

Figure 6-21: S_{31} (Coupled Port) vs. Frequency Simulation Result in Ensemble

6.6 Ansoft Ensemble Simulations Results of Complete Antenna System

The design of CDAR antenna is developed on Ensemble 8.0 simulation program. At the beginning of the thesis study, CDAR antenna is fed from two separate probes in simulations. After acquiring the desired simulation results for Power Pattern and Reflection (S_{11} result), the power divider structure is developed in ADS Software. Next, The Ensemble simulation results of the broadside coupler are also important, so, the broadside coupler is simulated in Ensemble program separately. At last step, the antenna layers and coupler layers are combined and whole system is simulated in Ensemble 8.0. The simulation results of the complete CDAR antenna system are given below.

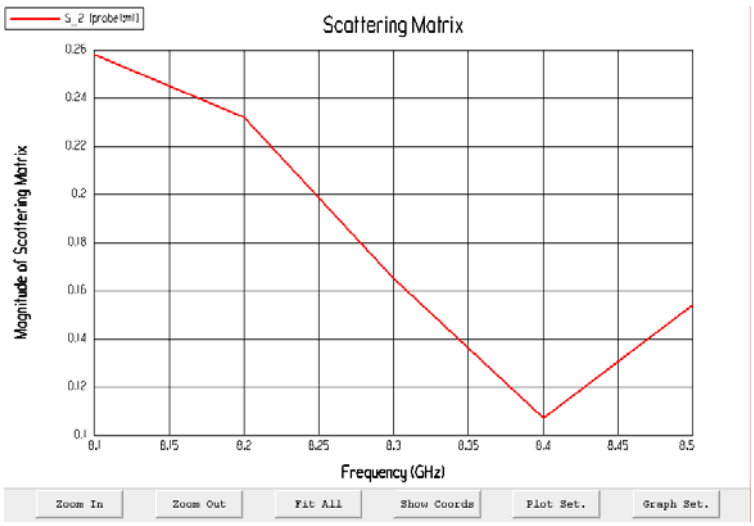

Figure 6-22: Ensemble simulation Result for Whole System S_{11} (Reflection)

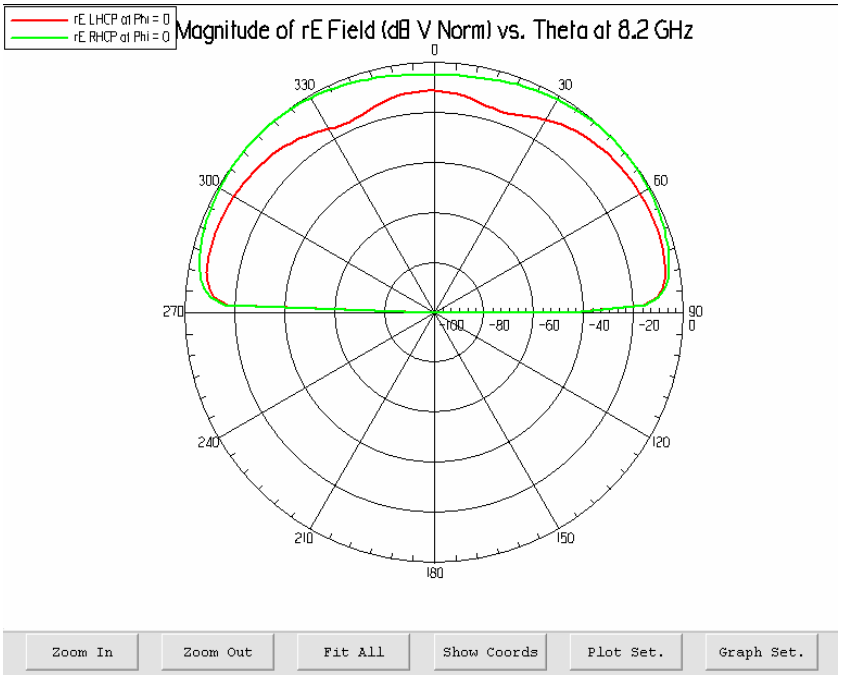

Figure 6-23: Ensemble simulation Result for Whole System Normalized rE Field in dB

CHAPTER 7

VERIFICATION OF THE THEORETICAL DESIGN MODEL

The full design processes of Single-Fed Circularly Polarized CDAR antenna are discussed in this thesis. A prototype of the CDAR antenna is produced and used in measurements. The prototype is basically composed of four different layer items which include one CDAR patch antenna radiator layer and three broadside coupler layers. The final product is measured in the laboratory by using special devices such as network analyzer, spectrum analyzer, and signal generator. The measured results are used to verify the theoretical design and the Ansoft Ensemble 8.0 Simulation program results. The measured results are interpreted and compared with theoretical results.

7.1 Circular Disk Annular Ring Antenna Production

As stated before, the CDAR antenna consists of four different layers. All layers are made by Rogers RO5880 dielectric substrate with $\varepsilon_r = 2.2$. However, the thicknesses of these substrates are different from each other. The patch antenna radiator layer thickness is $h = 1.57$ mm, and the broadside coupler layers have thicknesses of $h = 0.51$ mm, $h = 0.127$ mm, and $h = 0.51$ mm. These layers have physical connections through via holes. On the back side of the antenna structure, there is a single coaxial connector and one via hole which is terminated by 50Ω resistor. On the patch radiator layer, there are two via holes which transfer the power coming from the coupler layers to the radiator patches.

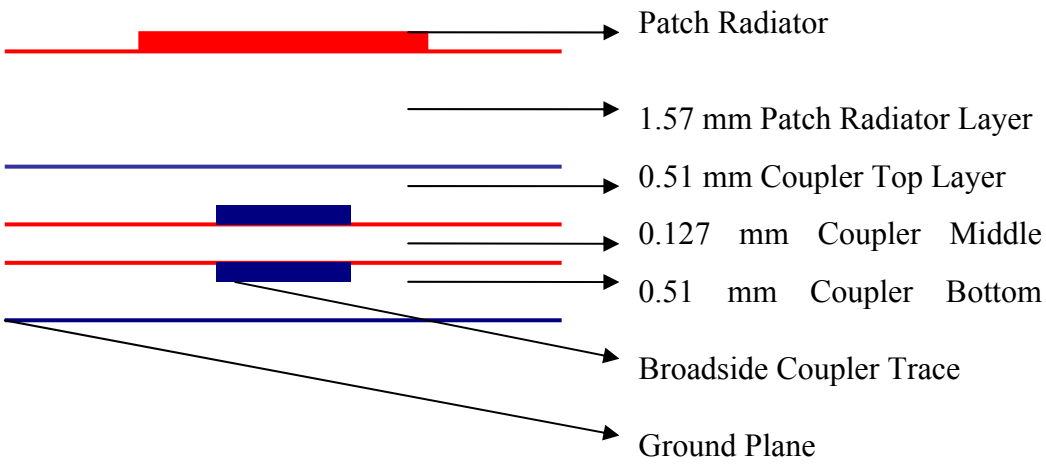

Figure 7-1: CDAR Antenna Layers

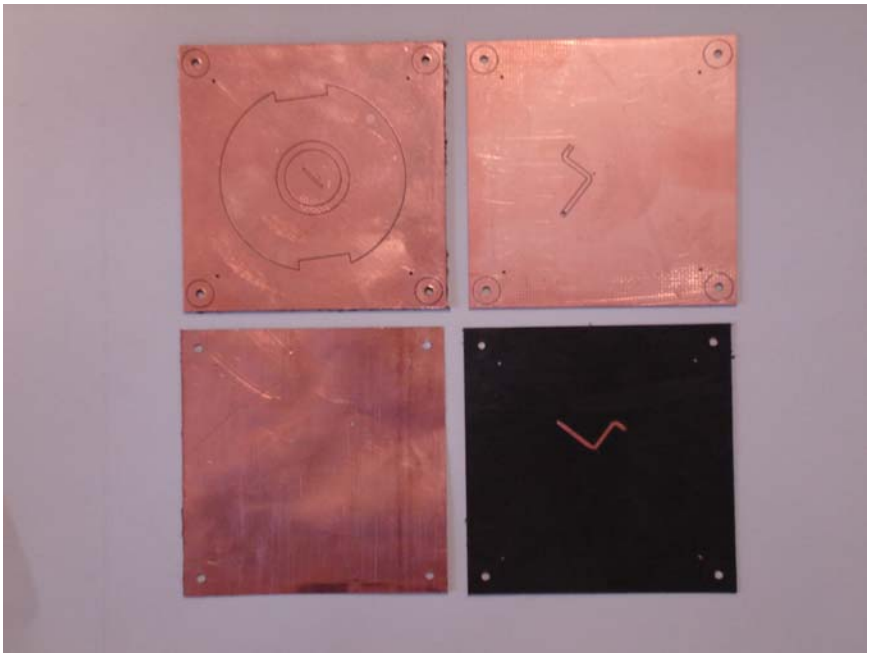

Figure 7-2: CDAR Antenna (Before Integration)

The size of the PCB is selected as 6 *X* 6 cm which is slightly larger than the outer diameter of the ring patch. Generally, the ground plane of the patch antennas should be three or four times bigger than free space wavelength λ_0 which is

nearly $13 \, X \, 13$ cm in this case. However in order not to waste much amount of Rogers RO5880 substrate, it is beneficial to produce small sized PCB and then, the ground plane is extended to the desired size using a regular conductor plate.

All layers are routed on LPKF machine by 0.2 mm router. The unwanted copper regions on the surface should be eliminated after routing process. The reason why the unwanted copper area was not scraped off by LPKF is that the router blade decreases the dielectric thickness of the substrate. To eliminate these undesired regions, hydrochloric acid is used. Before this process, the desired copper regions is dyed by a special pen and also covered by tape to protect these regions from dissolving.

After manufacturing process, the layers should be aligned and integrated carefully. To align these layers, four alignment and four screw points are drilled at the corners of each layer. At this stage, it is beneficial to connect all the ground planes from these alignment holes by conducting wires. However, because the via holes are not coated by copper, before integration process, one should solder very thin wires through the via holes and solder all the connection points. Then, to minimize the undesired radiation from these connection points, one should rub the soldering points by emery paper. When the alignment and soldering processes are finished, the ground plane is soldered to a 13 X 13 cm conductor plate to extend the ground plane size. On the back side of antenna, the coax connector is soldered to the ground plane from its all contact points to eliminate the undesired back radiation and increase the mechanical strength of the coax connector.

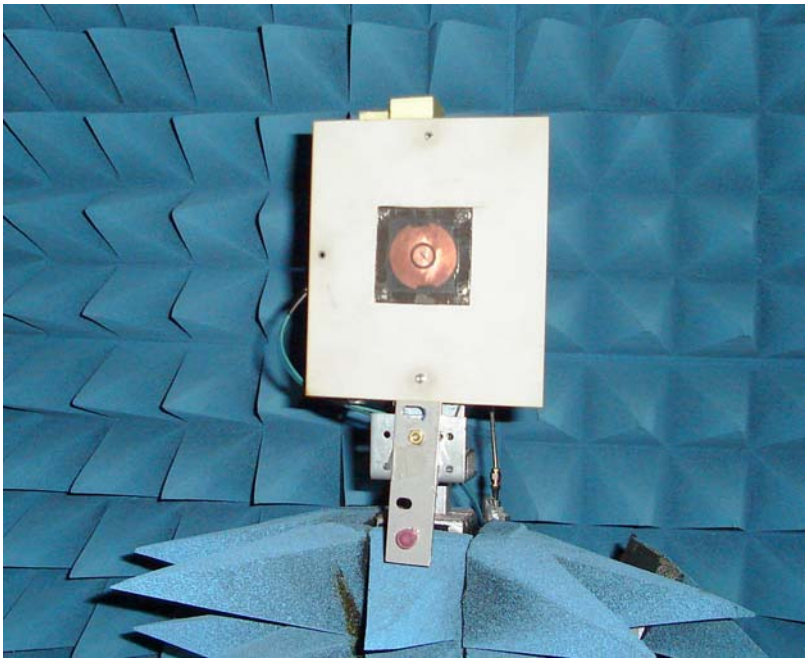

Figure 7-3: CDAR Antenna (Measurement Set-Up)

7.2 Measurements of the Antenna Parameters and Radiation Pattern

The basic parameters of an antenna that can be measured in the laboratory are:

- S_{11} value to evaluate the reflection at the input port
- Antenna radiation pattern
- Antenna Gain
- Type of Polarization

The first measurement is S_{11} parameter which gives the relation between the frequency and the reflection. The measurement is taken by using Network Analyzer. As one can see from the measured data on Figure 7-4, the best frequency that the input power is transferred to the radiator is nearly 8.25 GHz. At this frequency, the S_{11} value is -15.3 dB which means that the ratio of reflected power to the input power is nearly $\frac{1}{34}$. This result is considered as a good

matching condition. However, because the CDAR antenna is designed at resonant frequency of 8.2 GHz, one should look at the S_{11} value at this resonant frequency. The curser on S_{11} figure shows -13.5 dB value at resonant frequency which means that ratio of reflected power to the input power is nearly $\frac{1}{22.5}$. This matching point is enough to continue the measurements. On the same figure, the simulated S_{11} graph is given. The simulated graph resembles to the measured one. The only difference is that the frequencies are shifted to right by about 1.5 GHz and the power values are shifted nearly by 2 dB. This shift can be expected, because the solders points on the via holes and other manufacturing disorders may increase the reflection. However, as stated before, the prototype antenna has still good matching condition and one can continue to the other measurements.

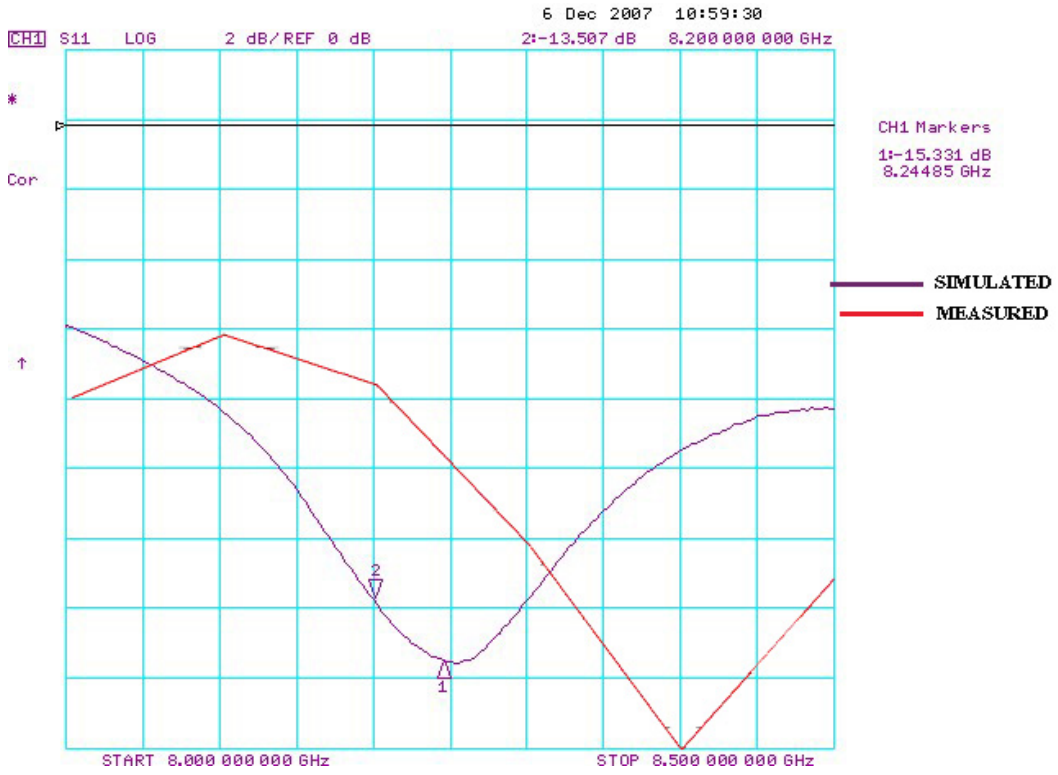

Figure 7-4: Simulated and Measured S11 Graph of CDAR Antenna

On Figure 7-5 and 7-6, normalized measured and simulated radiation patterns at $\phi = 0^o$ and $\phi = 90^o$ angle can be seen. The power level of the broadside angle is designed as 4 dB lower than the maximum power level. This is achieved on simulation results. However, the measured power level is nearly 8 dB lower than the simulated one at broadside angle. This unexpected situation may be because of the coupler. If one excites the ring patch by more power, the decrease on broadside angle gets bigger. From Figure 6-9 (Amplitude Constant vs. Decrease Level in Power Pattern in dB), one can say that if the CDAR antenna is excited by 3 dB coupler, the measured radiation pattern is occurred. In the manufacturing process, if the alignment of the arms of the coupler is not precise, the coupling ratio is affected, and the coupler may divide the input power equally if the offset between the arms is nearly 0.3 mm instead of 0.78 mm.

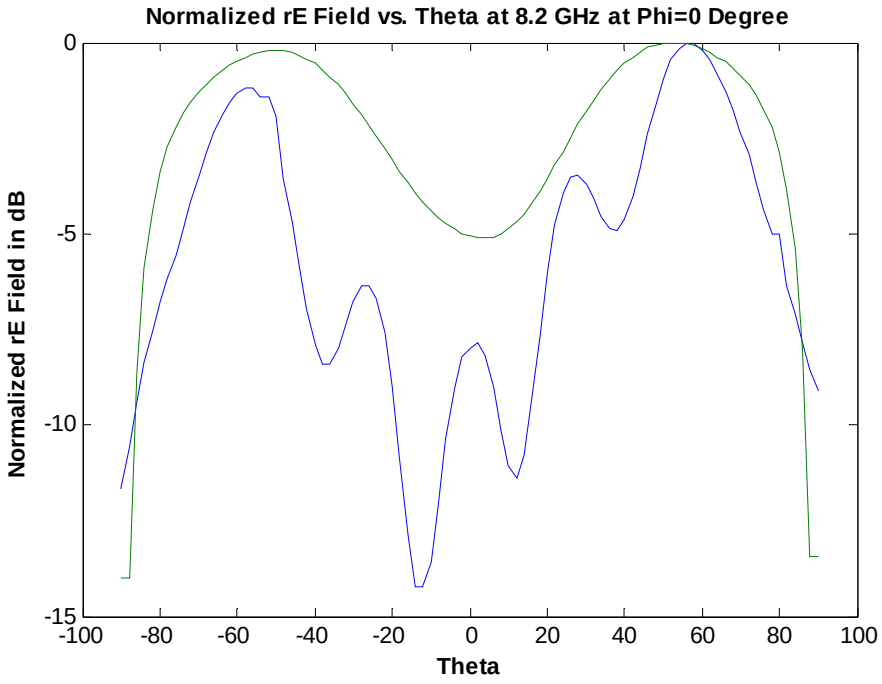

Figure 7-5: Normalized Measured and Simulated Radiation Pattern at $\phi = 0^o$ plane at the Resonant Frequency

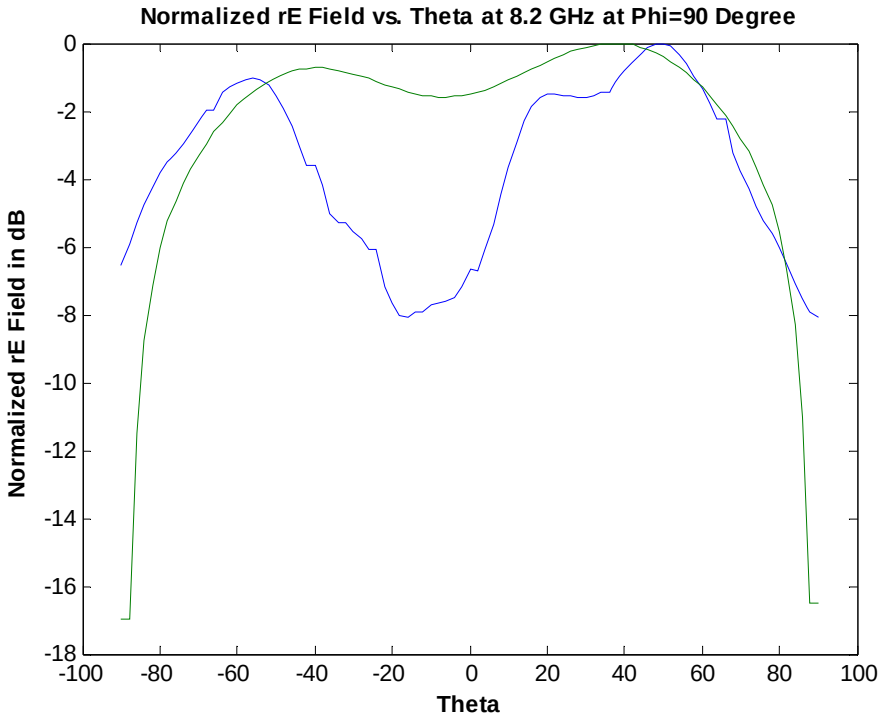

Figure 7-6: Normalized Measured and Simulated Radiation Pattern at $\phi = 90^o$ plane at the Resonant Frequency

Because of the single feeding points on the separate radiators, the radiation pattern is not symmetrical. On simulation results, the asymmetry between the main lobes is nearly 0.2 dB at $\phi = 0^o$ plane radiation pattern and 0.8 dB at $\phi = 90^o$ plane radiation pattern. This asymmetry is more pronounced on measured radiation patterns. The asymmetry is nearly 1 dB at $\phi = 0^o$ plane radiation pattern and 2 dB at $\phi = 90^o$. The reason of this result may also be the wrong coupling ratio as discussed on above paragraph.

The following figures are the simulated and measured radiation patterns at $\phi = 0^o$ at different frequencies.

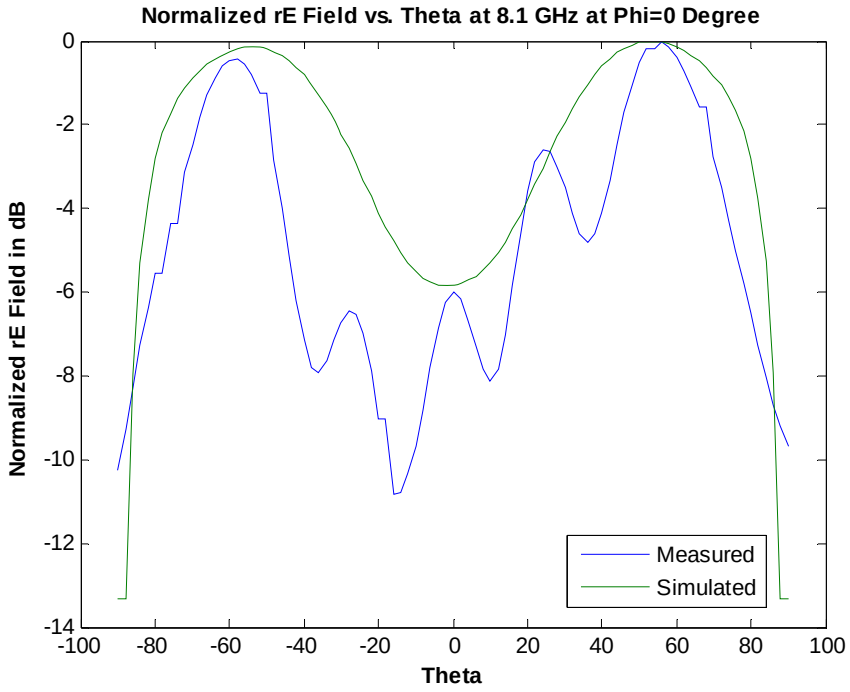

Figure 7-7: Normalized Measured and Simulated Radiation Pattern at $\phi = 0^o$ plane at 8.1 GHz

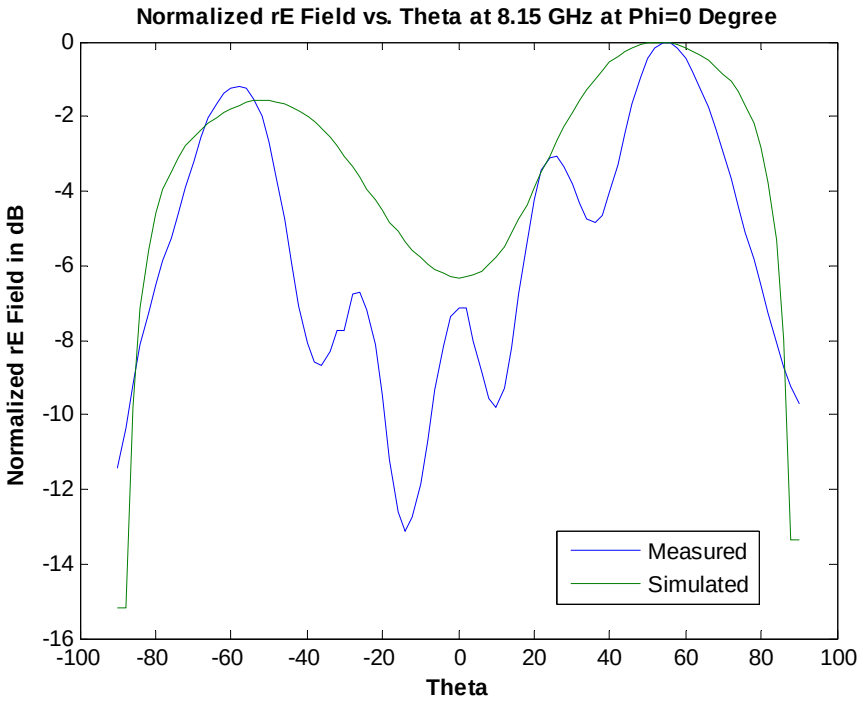

Figure 7-8: Normalized Measured and Simulated Radiation Pattern at $\phi = 0^o$ plane at 8.15 GHz

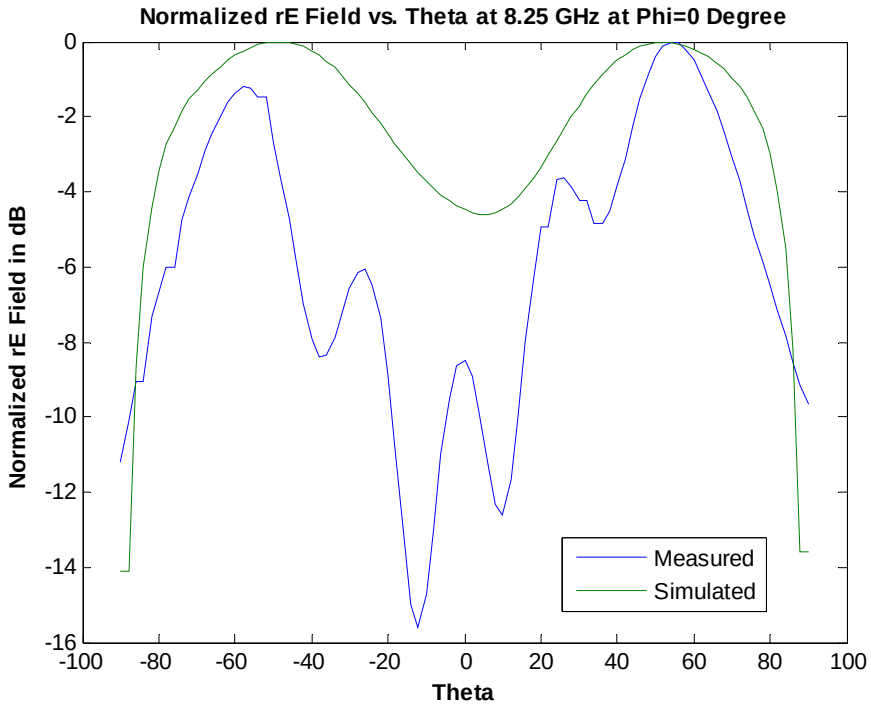

Figure 7-9: Normalized Measured and Simulated Radiation Pattern at $\phi = 0^o$ plane at 8.25 GHz

Another important figure of merit that describes the performance of an antenna is its gain. To measure the gain of an antenna, two different methods can be used. First one is to use two identical calibrated antennas. Two different measurements are taken in this method. Firstly, one of the calibrated antennas is the transmitter and the CDAR antenna is the receiver. Secondly, the receiver antenna is replaced by other identical calibrated antenna. After the measurements, the gain of the actual antenna can be calculated as:

$$P_1 = P_{in} + G_1 + G_2 + \left(\frac{\lambda}{4\pi R}\right)^2_{db}$$

$$P_2 = P_{in} + G_1 + G_1 + \left(\frac{\lambda}{4\pi R}\right)^2_{db}$$

then,

$$G_2 = P_1 - P_2 + G_1$$

where

P_1 is the first measured received power in dB

P_2 is the second measured received power in dB

P_{in} is the input power in dBm

G_1 is the calibrated antenna gain in dBic

G_2 is the CDAR antenna gain in dBic

The main advantage of this method is that the cable losses, amplification levels and other parameters do not affect the result. They all disappear after subtraction of the received powers from each other.

The other method can be used when the gain of the transmitter antenna is not known. In this method, one should get three different measurements such as:

- Antenna 1 is transmitter – CDAR antenna is receiver
- Antenna 1 is transmitter – Antenna 2 is receiver
- CDAR antenna is transmitter – Antenna 2 is receiver

Form these measurements, one can write the following expressions:

$$P_1 = P_{in} + G_1 + G_2 + \left(\frac{\lambda}{4\pi R}\right)^2_{db}$$

$$P_2 = P_{in} + G_1 + G_3 + \left(\frac{\lambda}{4\pi R}\right)^2_{db}$$

$$P_3 = P_{in} + G_2 + G_3 + \left(\frac{\lambda}{4\pi R}\right)^2_{db}$$

then,

$$2G_2 = P_1 + P_3 - P_2 - \left(\frac{\lambda}{4\pi R}\right)_{db}^2$$

where

P_1 is the first measured received power in dB

P_2 is the second measured received power in dB

P_3 is the third measured received power in dB

P_{in} is the input power in dBm

G_1 is the antenna-1 gain in dBic

G_2 is the CDAR antenna gain in dBic

G_3 is the antenna-2 gain in dBic

There is no calibrated circularly polarized antenna in the laboratory. So the gain measurements were made by using second method. However, because the setup is not perfectly lossless setup, one should consider the cable losses and amplifications. The cable losses are nearly -5 dB on both receiver and transmitter sides. The receiver is connected to 36.5 dB amplifier, all the measurements are made by 8 dBm input power, and the distance between transmitter and receiver antennas is nearly 5 m long. By using these parameters, one should change the gain expression as follows:

$$2G_2 = P_1 + P_3 - P_2 - \left(\frac{\lambda}{4\pi R}\right)_{db}^2 + Loss_{cable} + Loss_{cable} - Amplifier$$

where

$Loss_{cable}$ is the cable loss which is 5 dB

$Amplifier$ is the amplification on receiver side that is 36 dB

$\left(\frac{\lambda}{4\pi R}\right)_{db}^2$ is the free space attenuation that is -63.89 dB

then the gain is calculated as:

$$2G_2 = -10.37 - 39.9 + 26.4 + 63.89 + 5 + 5 - 36.5 \cong 14.32 \Rightarrow\Rightarrow G_2 = 6.76 \text{ dBi.}$$

The measured gain is very different from the simulation result which is nearly 3.9 dBi. There are two basic reasons for this difference. First one is setup is not perfectly calibrated and the losses used in the equations are not the actual values. So, the measured gain is not accurate, however it is obvious that the gain is greater than 6 dBic. The second reason is that the measured power level at the broadside angle is much more than the simulated one. It is obvious that the more decrease at the broadside angle, the more increase on the gain of the antenna.

The last measurement is the type of polarization. Figure 7-10 shows the simulated axial ratio at resonant frequency.

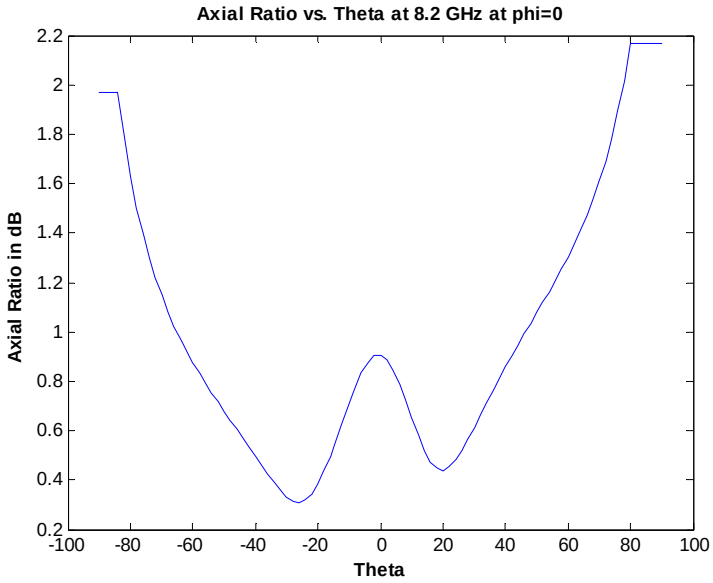

Figure 7-10: Simulated Axial Ratio vs. Theta at $\phi = 0^o$ plane at the Resonant Frequency

The polarization of an antenna can be tested as the receiver antenna is rotated around its own x-y plane. Then the received power graph gives the polarization

curve. For circularly polarized antenna, the polarization curve is a circle. However, in the laboratory, the setup does not support this kind of computer controlled rotation. By taking measurement on the angle values such as 0°, 15°, 30°, 45°, 60°, 75°, 90° degrees, the polarization curve can be formed. The following table shows the received power values at broadside angle at the given theta values. The antenna is not perfectly circularly polarized; however, the CDAR antenna satisfies the requirements of circular polarization.

Table 7-1: Power Levels at Different Angle

Theta Angles	Normalized Power Values at Broadside Angle
0°	1,29 dB
15°	1,06 dB
30°	1,02 dB
45°	1,52 dB
60°	1,19 dB
75°	0 dB
90°	0,14 dB

CHAPTER 8

CONCLUSION

On this report, design of Single-Fed Circularly Polarized CDAR antenna is investigated considering its all design, manufacture and test steps. This microstrip antenna structure is new in the literature. The combination of circular disk and annular ring patch antennas are generally researched as dual-band patch antennas. However, in this thesis, CDAR antenna is studied to achieve special power pattern for LEO satellite communication. In brief, there are no studies on this antenna structure and the study on this thesis is helpful to researchers who want to study on singly-fed circular polarization on patch antennas, LEO satellite communication antennas and power dividers and/or couplers.

In this report, the full design procedure of CDAR antenna from the theoretical background and mathematical equations to the manufacturing and test processes is given. The theoretical background starts by super position of two different antenna patterns to give the desired LEO Satellite power pattern. Then the mathematical analysis of these two types of antennas and their super position are investigated. After this point, the Ansoft Ensemble 8.0 Simulation program is used to simulate the designed antenna system. Up to now, the design is not circularly polarized. Perturbation method is used to achieve the singly-fed circular polarization. Feeding structure of the patch antenna and coupler model for required power division are also developed and presented on this report by comparing different types of coupler and feeding structures.

At the end of the thesis study, a prototype of CDAR antenna is manufactured and tested to verify the theoretical design. The matching properties and other antenna parameters such as power pattern, gain and polarization are consistent with the simulation results. One can claim that this antenna model is successful and highly

satisfactory to use in LEO satellites. However further studies should be done such as selecting space compatible substrate, new mechanical design for placement on satellite and testing the compatibility to space environment.

REFERENCES

[1]. C. W. Bostian and V. W. Chan, Review Assessment Of Satellite Communications Technologies

[2]. M. Taştan, Analysis and Design of A Circularly Polarized Microstrip Antenna, METU, 2006.

[3]. I. J. Bahland and P. Bhartia, Microstrip Antennas, Artech House, Dedham, MA, 1980.

[4]. J. R. James and P. S. Hall, Handbook of Microstrip Antennas, Vols. 1 and 2, Peter Peregrinus, London, UK, 1989.

[5]. J. Huang, Circularly Polarized Conical Patterns from Circular Microstrip Antennas, IEEE Trans. on Antennas and Propagation, vol. Ap-32, no. 9, september 1984, pp. 991-994.

[6]. E. Akgün, Millimeter Wave Microstrip Launchers And Antenna Arrays, METU, 2006

[7]. Balanis, Constantine A., Antenna Theory, Analysis and Design (2nd Ed), John Willey, 1997

[8]. Rogers Corporation, "RT/Duroid® 5870 /5880 High Frequency Laminates," http://www.rogerscorporation.com/mwu/pdf/5000data.pdf, August 2004, Last Accessed at December 2007.

[9]. Rogers Corporation, "Design Equations for Broadside and Edgewise Stripline Couplers," http://www.rogerscorporation.com/mwu/pdf/rt321.pdf, 2003, Last Accessed at December 2007.

[10]. "Branchline couplers" http://www.microwaves101.com/encyclopedia/Branchline_couplers.cfm, March 3, 2007, Last Accessed at December 2007.

[11]. "Quadrature couplers" http://www.microwaves101.com/encyclopedia/Quadrature_couplers.cfm, April 9, 2005, Last Accessed at December 2007.

[12]. "Couplers and splitters" http://www.microwaves101.com/encyclopedia/couplers.cfm, November 11, 2005, Last Accessed at December 2007.

[13]. A. K. Bhattacharyya and Garg R., Input Impedance of Annular Ring Microstrip Antenna Using Circuit Theory Approach, IEEE Trans. on Antennas and Propagation, vol. Ap-33, no. 4, Apr. 1985, pp. 369-374

[14]. W. H. KUMMER, GILLESPIE E. S., Antenna Measurements- 1978, Proceedings of the IEEE, vol. 66, no. 4, April 1978, pp. 483-506

[15]. D. M. Kokotoff, Aberle J. T., and Waterhouse R. B., Rigorous Analysis of Probe-Fed Printed Annular Ring Antennas, IEEE Trans. on Antennas and Propagation, vol. 47, no. 2, Feb. 1999, PP. 384-388

[16]. Y. T. Lo and S. W. Lee, Antenna Handbook Theory Applications and Design, Van Nostrand Reinhold Company, United States of America, 1988.

[17]. W. L. Stutzman and G. A. Thiele, Antenna Theory and Design, John Wiley & Sons, United States of America, 1981.

[18]. GRIFFIN, J. M., and FORREST, J. R.: 'Broadband circular disc microstrip antenna', Electron. Letts., 18 Mar. 1982, pp. 266-269.

[19]. FONG, K. S., PUES, H. F., and WITHERS, M. J.: 'Wideband multilayer coaxial-fed microstrip antenna element' ibid. 23 May 1985, pp. 497-499.

APPENDIX A

Antenna Gain Measurement

The techniques that are employed for the determination of the power gain of an antenna are dependent upon its frequency of operation. Above 1 GHz, for example, free-space antenna ranges are commonly available for gain measurements. For these frequencies, microwave techniques can be employed, since waveguide devices, including electromagnetic horns, are readily available. For frequencies between 0.1 and 1 GHz, ground-reflection ranges are usually required because free-space conditions are difficult to simulate. Because of the longer wavelengths, microwave techniques become less practical at these frequencies. Antennas operating in this frequency range are often mounted on structures, such as aircraft, which affect their characteristics. For these cases, scale modeling techniques may be employed. Since it is impractical to scale the finite conductivities and loss factors of the materials of which the antenna and aircraft are constructed, power-gain measurements cannot be performed using the scale model. However, the measured directivity of the model antennas will be equal to that of the full-scale antenna to accuracy commensurate with the accuracy with which the model was constructed and measured. If the efficiency of the full-scale antenna can be determined by other means, then the power gain of the full-scale antenna can be determined since the maximum power gain is equal to the product of the efficiency and directivity of the antenna. It is good practice to verify the results by requiring the aircraft, with the full-scale antenna mounted, to fly a prescribed path relative to a suitable ground station. The system performance, using the full-scale test antenna, can be measured and compared to that predicted from the scale model measurements. As the frequency is decreased below 0.1 GHz, the effect of the ground upon the antenna characteristics becomes increasingly pronounced, making power-gain measurements very difficult. Directive antennas at these lower frequencies are physically large and must be measured in situ. Often it is satisfactory for one to calculate the antenna gain and

estimate the effect of the ground. Again, scale models can be employed; however, because of the strong effect of the ground on the characteristics of the antenna, the electrical properties of the ground must also be scaled. For frequencies below about 1 MHz, the antenna power gain is not usually measured, but rather it is the field strength of the ground wave radiated by the antenna which is measured. For those frequencies for which power-gain measurements are practical, there are two general categories into which the various methods can be placed. They are: absolute-gain measurements and gain-transfer measurements. For an absolute-gain measurement, no u priori knowledge of the gains of any of the antennas used in the measurement is required. This method is usually employed for the calibration of antennas that are to be used as gain standards. The gain-transfer method, also referred to as the gain comparison method, is the most commonly employed method for power-gain measurements. This method requires the use of a gain standard to which the gain of the test antenna is compared [14].